UNITED NATIONS UNIVERSITY
UNU-GTP
Geothermal Training Programme

Orkustofnun, Grensasvegur 9,
IS-108 Reykjavik, Iceland

Reports 2018
Number 23

PROCESS DESIGN OF MICRO HYDRO, EXPANDER, BINARY ORC AND DOUBLE FLASH CYCLE USING SEPARATOR PRESSURE OF UNIT V IN LAHENDONG GEOTHERMAL FIELD, INDONESIA

Adhiguna Satya Nugraha
PT Pertamina Geothermal Energy
Area Lahendong, Jalan Raya Tomohon No. 420, Tomohon 95431
Sulawesi Utara
INDONESIA
adhiguna.nugraha@pertamina.com; adhiguna.nugraha24@gmail.com

ABSTRACT

The saturated liquid discharged from the production separator has the potential to drive a secondary turbine in Lahendong and other fields of the PT Pertamina Geothermal Energy company. The water from the separator flows directly to the reinjection wells due to a difference in elevation of about 60 metres. From well testing during the project's initial phase in 2012, and tracer flow tests in 2016 and 2017, the flow rates of steam and brine are known. Four different ways to recover energy from this saturated liquid flow stream before re-injection are studied in this project. First is to let the saturated liquid run through a micro hydro turbine (Pelton type) with a working pressure of 8.63 bar-a (head substitute), temperature 174°C, flow rate 40.6 kg/s and proportion of flash steam inside the pipe 0.13%. Under the assumption that no flashing or boiling occurs, the resulting power would be 32.06 kW. Second option is to insert the boiling liquid into a two-phase expander (turbo expander type) and a biphase turbine. The turbo expander generates about 282.2 kW electricity with an outlet pressure of 5.92 bar-a. The biphase turbine produces 9 kW at atmospheric pressure (0.924 bar-a) as the outlet pressure. This type of turbine can remove the vapour energy from the system. The third and most economic option would be the use of a binary ORC either with a wet or dry cooling tower. The calculation using Scilab and CoolProp for numerical computations resulted in a net power of 1795.3 kW with Silica Saturation Index, *SSI,* value of 2.02 and 626.1 kW with *SSI* value of 0.99 (with an existing wet cooling tower as the cooling system). Fourth option is a double-flash cycle with a differential pressure of 3.8 bar-a which would produce 2447.6 kW.

1. INTRODUCTION

The Lahendong geothermal field is in North Sulawesi in Indonesia and is part of the PT Pertamina Geothermal Energy (PT PGE) working areas (Figure 1). PT Pertamina Geothermal Energy is a subsidiary company of PT Pertamina (Persero) and PT Pertamina Dana Ventura whose aim is to develop geothermal energy as a renewable energy, including all processes upstream to downstream both on a national and international level. In 2018, the total capacity of geothermal production in the Lahendong

FIGURE 1: Location of Lahendong geothermal field (6 × 20 MW), North Sulawesi, Indonesia (PT PGE, 2018a)

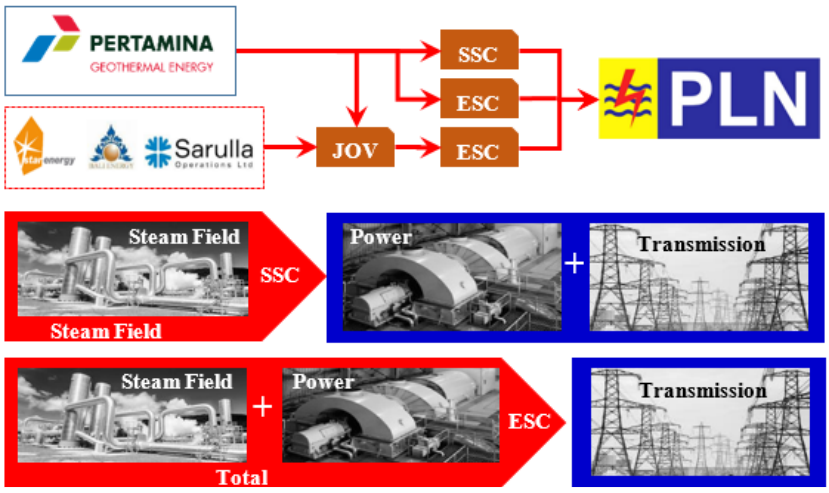

FIGURE 2: Business schemes of PT Pertamina Geothermal Energy (PT PGE, 2018b)

field was 120 MW (PT PGE, 2018a) which consists of 6 power plant units. Units I to IV with a total production capacity of 80 MW are in Lahendong while Units V to VI are located in the 18 km distant Tompaso area.

Figure 2 shows two business schemes of PT Pertamina Geothermal Energy for developing fields. The first scheme is a steam sales contract. It covers the upstream side or steam field while the downstream side is covered by National Electricity Company, PT PLN (Persero). This refers to Units I to IV in Lahendong. The second scheme is called an electricity sales contract that extends to the downstream side (total project) and refers to Units V-VI, while the National Electricity Company is handling the grid and distribution.

1.1 Background information

The Lahendong Units V and VI geothermal fields have an elevation of 789 m a.s.l. and the average atmospheric pressure is 0.924 bar-a. The production wells are located at an elevation of about 790 m above sea level while the reinjection wells are at an elevation of around 723 m a.s.l. The geothermal fluid is two-phase, and the field consists of one cluster of production wells as well as two clusters of reinjection wells:

1. *Production wells (Cluster 27):*
   LHD-27; LHD-31; LHD-34; LHD-42; and LHD-43.

   Three of the production wells LHD-27, LHD-31, and LHD-34 supply steam to power plant Unit V, while the other two supply steam to power plant Unit VI.

2. *Reinjection wells (Cluster R):*
   Cluster R-1: LHD-41; and LHD-46.
   Cluster R-2 LHD-40; and LHD-44.

   The reinjection wells maintain the water level in the reservoir. Cold brine is pumped from thermal ponds to the reinjection wellhead and/or to the main reinjection line before entering to the reinjection wellhead. The ponds' function is to collect steam condensate that occurs in the pipeline systems due to pressure drop. It also collects water that is discharged from the separator through a pneumatic emergency dump valve if the water level becomes to high (overflow).

1.2 Well testing result in Unit V wells

Well testing was carried out in Lahendong to obtain the flow rate of fluids. The aim was to determine the possible power generation with as a function of well head pressure to optimize design and construction in the geothermal facilities. The separator method was used in order to acquire a more accurate result. For fluid flow rate and enthalpy values with various wellhead pressure settings see Figure 3. The separator pressure setting during the well tests is controlled by three internal programs:

LHD-27 = ± 10 barg of separator pressure with maximum discharge pressure 27.95 barg;
LHD-31 = ± 8 barg of separator pressure with maximum discharge pressure 18.14 barg; and
LHD-34 = ± 10 barg of separator pressure with maximum discharge pressure 32.36 barg.

Based on the results from the separator method, the optimum wellhead pressure for LHD-27 is 13.73 barg with the valve opened about 30%, then the steam fraction can reach 18.49% (PT PGE, 2012a). The optimum wellhead pressure setting of LHD-31 is 16.67 barg with valve opened 11%, the steam fraction reaches 12.35% (PT PGE, 2016) and for LHD-34 it is 22.56 barg with valve opened 50%, the steam fraction reaches 20.59% (PT PGE, 2012b).

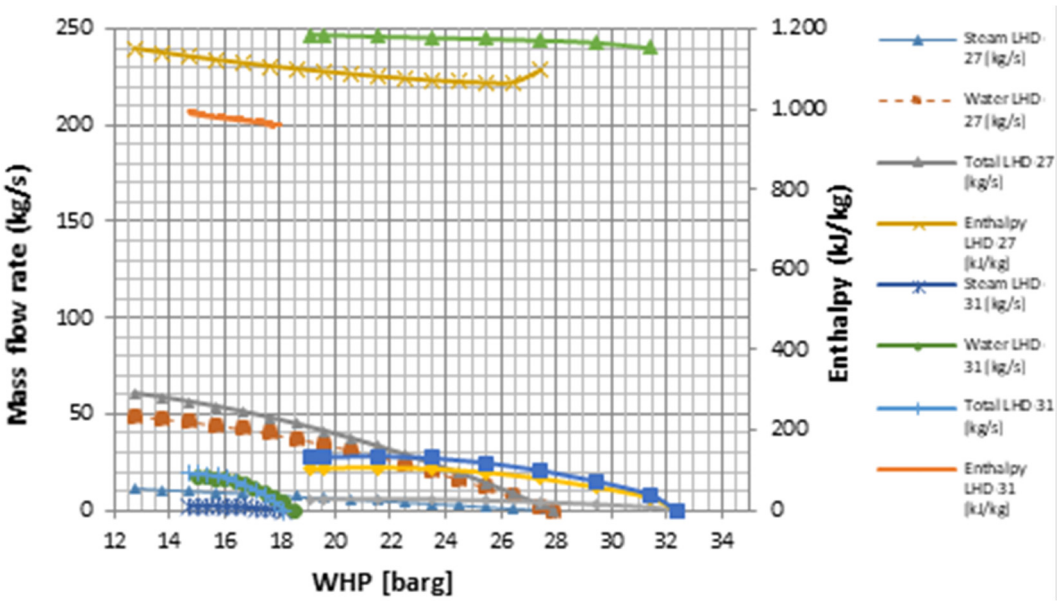

FIGURE 3: Deliverability curves of Lahendong Unit V wells

1.3 Tracer flow test result in Unit V and VI wells

The steam and water flow rates have been measured with tracer flow tests in 2016 and 2017 as shown in Table 1. The setting of the wellhead pressure is based on the well testing. However, the results obtained during well testing and the tracer flows test show different flow rates because of pressure setting in the separator.

TABLE 1: Tracer flow test result of Unit V and VI wells (PT PGE, 2017)

Well	Date	WHP (barg)	Throttle open (%)	Steam	Water	Total	Enthalpy (kJ/kg)	Dryness (%)
				ton/hr				
Unit V wells								
LHD-27	3 Oct 2016	16.90	25	45.72	192.96	238.68	1118.20	19.18
	21 Apr 2017	16.70	24	26.90	190.13	217.03	1114.70	12.39
	23 Oct 2017	15.89	24	39.85	176.80	216.65	1123.16	18.39
LHD-31	4 Oct 2016	15.50	28	45.72	344.52	390.24	965.80	11.72
	21 Apr 2017	14.57	28	35.40	223.43	258.83	1116.80	13.68
	23 Oct 2017	13.91	28	40.82	248.95	289.77	1037.78	14.09
LHD-34	3 Oct 2016	31.40	23	57.60	241.92	299.52	1118.70	19.20
	21 Apr 2017	29.88	30	94.80	299.61	394.41	1442.50	24.04
	23 Oct 2017	29.24	36	69.82	252.45	322.27	1191.02	21.67
Unit VI wells								
LHD-42	22 Apr 2017	15.16	18	39.94	196.08	236.02	1188.20	16.92
	22 Oct 2017	13.19	25	58.95	204.89	263.84	1192.91	22.34
LHD-43	22 Apr 2017	19.21	77.50	100.30	430	530.30	1262.70	18.91
	22 Oct 2017	19.67	71	110.50	398.75	509.25	1191.70	21.70

2. STUDY DESCRIPTION

2.1 General overview

The process flow diagram of Units V and VI in Figure 4 below describes how the two-phase fluid from the five production wells is transported to the power plant. The fluids are separated in the separator vessel. For power generation in Unit V, the geothermal fluids from three production wells (LHD-27, LHD-31, LHD-34) are transported to separator A. The fluid from the production wells LHD-42 and LHD-43 is transported to separator B. The separated steam from each separator is transferred to the scrubber vessel in order to remove any remaining liquid/condensate and from there the dry steam from the scrubber is forwarded into two 20 MW turbines. In case of shortage of supply to one of the seperators, an interconnecting pipe can be opened to redirect some of th fluid. The separated water from separator station A and B is directed to the reinjection header line then mixed with condensate if necessary. The collected fluids are then transported to the four reinjection wells.

The pressurised water and hot water inside pipe from the separator outlet can potentially be utilized. The pressurised water will be redirected towards to the hydrothermal turbine. The mixture of water and vapour discharged by the turbine will go into the thermal pond and is then pumped to the reinjection wells.

The operation and production parameters of Unit V and VI at design condition are shown in Table 2.

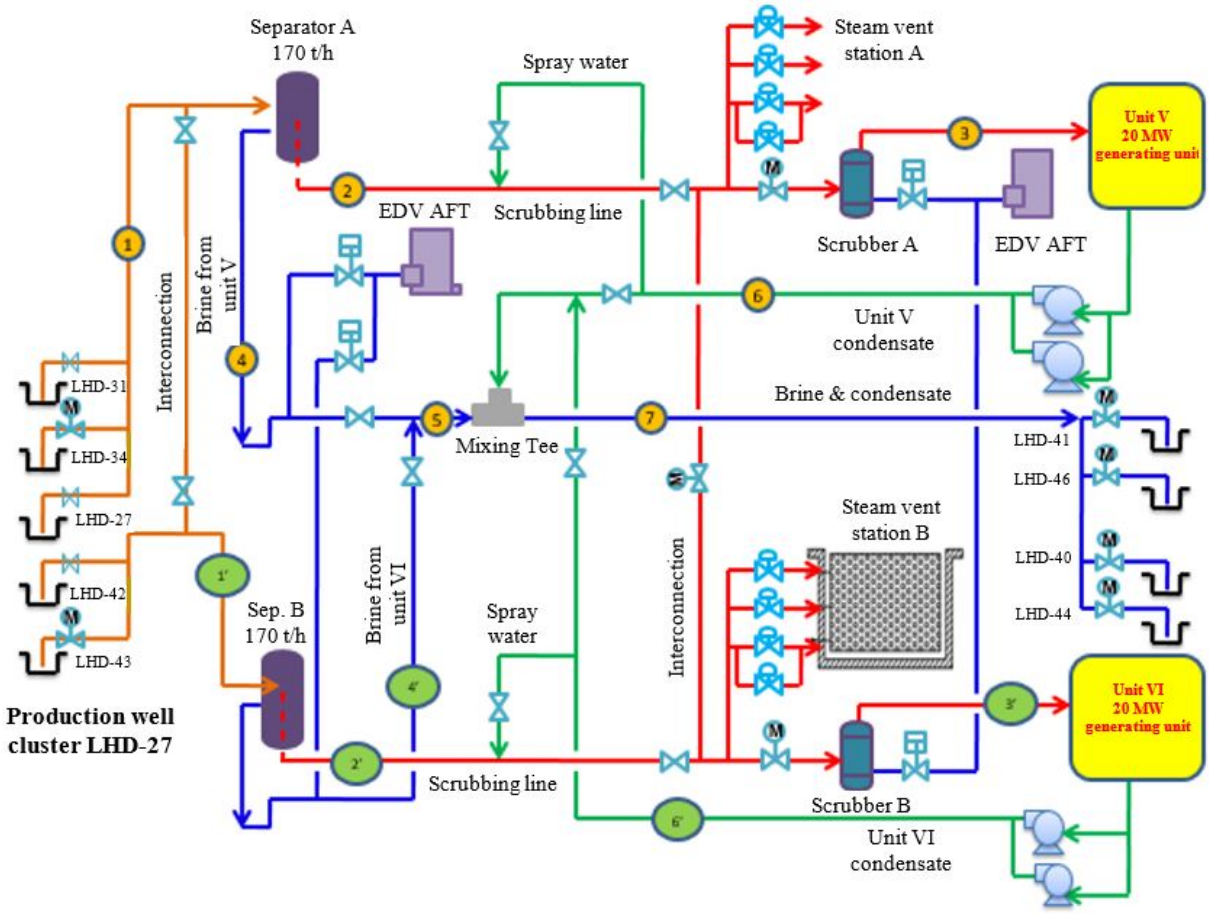

FIGURE 4: Flow diagram of Units V and VI in Lahendong geothermal field

TABLE 2: Operation and production parameters of Lahendong Unit V and VI at design condition

No.	Description	Unit	Stream number					
			1	1”	2	2”	3	3”
1.	Pressure	bar-a	8.90	8.870	8.60	8.57	8	8
2.	Temperature	°C	174.90	174.70	173.40	173.30	170.20	170.20
3.	Enthalpy	kJ/kg	1118.90	1118.40	2767.10	2767.00	2768.12	2768.12
4.	Mass flow rate	ton/hr	716.10	716.10	135.20	135.20	133.11	133.11
		kg/s	180.45	180.45	34.07	34.07	33.54	33.54
No.	**Description**	**Unit**	**Stream number**					
			4	**4”**	**5**	**6**	**6”**	**7**
1.	Pressure	bar-a	8.60	8.60	8.80	13	13	12.90
2.	Temperature	°C	174.40	173.30	173.30	38.50	38.50	164.30
3.	Enthalpy	kJ/kg	734.20	733.60	738.20	162.50	162.50	694.80
4.	Mass flow rate	ton/hr	580.90	580.80	1161.70	39.50	39.50	1240.70
		kg/s	146.38	146.36	292.74	9.95	9.950	312.65

The total amount of two-phase fluids passing through the separators is about 180.45 kg/s each, at a pressure setting of the separators at 8.9 and 8.87 bar-a, respectively. The steam flows toward the turbine with an inlet pressure of 8 bar-a and 34.07 kg/s flow rate. The separated water has a flow rate of 146.38 kg/s from separator A and 146.36 kg/s from separator B with working pressure 8.6 bar-a. However, the water from both separator vessels would be mixed in the reinjection pipe header and the line pressure increases to 12.9 bar-a due to the elevation difference of around 60 m between the production and the

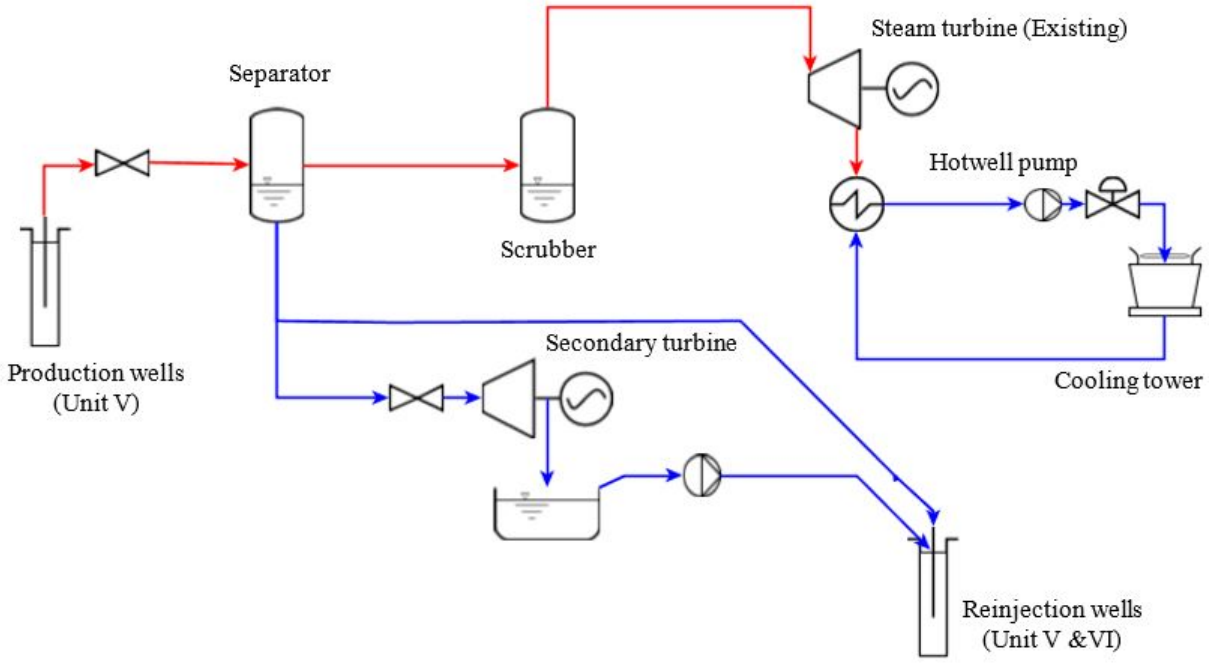

FIGURE 5: Schematic diagram of micro hydro and hydrothermal turbine

reinjection wells. The average steam fraction (dryness) from the wells is 18.88%. The existing production facility will have to be modified (Figure 5).

2.2 Objective of the study

The aim and objectives of this study are:

1. To design and analyse a hydro power (either cold or hot) binary ORC and double-flash cycle turbine using pressurised water and saturated liquid inside pipe before the fluids flows to the reinjection wells;
2. Provide an alternative solution to the design and development of hydro power, binary turbines and double-flash cycles in geothermal fields;
3. To substitute the high elevation and water pond/dam required to acquire water flow into the hydro turbine;
4. Developing a production facility process that can provide added economic value;
5. To obtain the auxiliary power from utilization the kinetic energy of fluids for own use electricity or house load purposes in Lahendong and Tompaso geothermal field in the future; and
6. Reduce cost of electricity consumption from the National Electricity Company (steam field project scheme) or optimizing export of electricity to the grid (total project scheme).

2.3 Scope and limitations of the study

The calculations in this report concern pipe design, pressure drop analysis, heat loss analysis, micro hydro and hydrothermal turbine selection, binary power design, double-flash cycle as well as silica saturation index. The study is limitatedto the potential of Unit V of the Lahendong geothermal field, especially regarding the two-phase system, using the present working pressure of separator and saturated liquid flow rate inside pipe.

2.4 Collection of data

This paper will be referring to existing data:

1. Operation and production data. During operation data is collected from the Lahendong geothermal field, the data is monitored and recorded at a central control room by a DCS (Distributed control system) device;
2. Tracer flow test and fluids sampling result. Tracer flow tests were carried out to estimate flow rates and the analysis of fluid samples indicates the possibility of scaling during the operation.; and
3. Related literature. Books, journals, articles, and electronic media were consulted in questions of engineering and design concepts.

3. THEORETICAL BACKGROUND

3.1 Pipe design

To determine the pipe size that best fits the fluid and the process, the physical properties of fluids as well as the material properties of the pipe must be known. The cross-sectional area of the pipe can be obtained with the following equation:

$$A = \frac{1}{4} \cdot \pi \cdot D_{in}^2 \tag{1}$$

Fluid velocity inside of a pipe is:

$$V = \frac{m}{A \cdot \rho} \tag{2}$$

where A = Cross sectional area (m^2);
V = Fluid velocity (m/s);
D_{in} = Inner diameter of pipe (m);
m = Mass flow (kg/s);
ρ = Fluids density (kg/m^3).

For the recommended fluid velocity see Table 3.

TABLE 3: Recommended fluid velocity (Lyle, 1947)

No.	Fluid	Type	Min	Max	Unit
1.	Two-phase	Exhaust steam (wet)	21	31	m/s
2.	Saturated	Dry saturated steam	31	40	m/s
3.	Superheated	Superheated steam	46	61	m/s
4.	Single water	Water	1.22	2.44	m/s

The pipe thickness as a function of pressure, according to ASME B 31.1 Power Piping (American Society of Mechanical Enginers - ASME, 2000a), is:

$$t_r = \frac{P \cdot D}{2 \cdot (S \cdot E + P \cdot Y)} \tag{3}$$

$$t_m = t_r + CA \tag{4}$$

where t_r = Pipe thickness required (mm);
t_m = Pipe thickness minimum (mm);
P = Working pressure (Psi);

D = Outside diameter of pipe (inch);
S = Allowable stress of material (Psi);
E = Weld joint efficiency factor, 1 for seamless pipe and 0.85 for Electric Resistance welded (ERW) pipe;
Y = Yield strength of material
CA = Corrosion allowance (mm).

3.2 Pressure drop analysis

The pressure drop is defined as the difference in total pressure between the start and the end points of a pipeline system. The frictional forces that the fluids experiences create pressure drop and depend on fluid velocity and fluid viscosity.

The Reynolds number is calculated with Equation 5:

$$Re = \frac{\rho \cdot V \cdot D_{in}}{\mu} \tag{5}$$

Equation 6 (Darcy friction factor) and Equation 7 (Swamee-Jain equation) can be used to calculate the Darcy-Weisbach friction factor for a full-flowing circular pipe which approximates the implicit Colebrook-White equation (Jónsson, 2018).

$$Re \leq 2100, \qquad \mathrm{f} = \frac{64}{Re} \tag{6}$$

$$Re > 2100, \qquad \mathrm{f} = \frac{0.25}{\left(log_{10} \left[\frac{\epsilon}{\frac{D_{in}}{3.7}} + \frac{5.74}{Re^{0.9}} \right] \right)^2} \tag{7}$$

where *Re* = Reynolds number;
f = Friction factor;
μ = Fluids viscosity (kg/ms); and
ϵ = Absolute rougness (m).

In order to calculate the friction head, the second equivalent length is calculated using Equation 8:

$$L_e = L_p + n_b \cdot h_b \cdot D_{in} + n_c \cdot h_c \cdot D_{in} + n_u \cdot h_u \cdot D_{in} + n_v \cdot h_v \cdot D_{in} \tag{8}$$

where L_e = Equivalent length (m);
L_p = Pipe length (m);
n = Number of fittings, valve and other pipe connections;
h_b = Equivalent length of bends;
h_c = Equivalent length of connections, flow straight through;
h_u = Equivalent length of expansion units; and
h_v = Equivalent length of gate valve fully open.

The friction head can be calculated by:

$$H_f = \frac{f \cdot V^2 \cdot Le}{2 \cdot g \cdot D_{in}} \tag{9}$$

Then the pressure drops due to friction along of pipeline and the elevation difference can be explained by:

$$\Delta P_f = \rho \cdot g \cdot H_f \tag{10}$$

$$\Delta P_H = \rho \cdot g \cdot (Z_s - Z_e) \tag{11}$$

Furthermore, the total of pressure drop along the pipeline system can be summarized:

$$\Delta P_t = \Delta P_f + \Delta P_H \tag{12}$$

where H_f = Friction head (m);
ΔP_f = Pressure drop due to the friction loss (bar);
ΔP_H = Pressure drop due to the elevation difference (bar);
ΔP_t = Total pressure drop (bar); and
$Z_{s/e}$ = Elevation of start/end point (m).

Since the hot water pipe running off the separator will be attached to a new pipeline, we can use the Bernoulli's principle:

$$P_1 + \frac{1}{2} \cdot \rho \cdot V_1^2 + \rho \cdot g \cdot h_1 = P_2 + \frac{1}{2} \cdot \rho \cdot V_2^2 + \rho \cdot g \cdot h_2 \tag{13}$$

The proportion of flash steam is defined as:

$$x = \frac{(h_f \text{ at } P_1) - (h_f \text{ at } P_2)}{(h_{fg} \text{ at } P_2)} \tag{14}$$

where $h_{1/2}$ = Elevation (m^2);
x = Steam fraction (%);
h_f = Enthalpy of saturated liquid (kJ/kg);
h_g = Enthalpy of saturated vapour (kJ/kg); and
h_{fg} = Latent heat of evaporation (kJ/kg).

3.3 Heat loss analysis

According to Fourier's law, the calculation of heat transfer by conduction through the pipe wall is as follows (hollow cylinder):

$$q = -\frac{kA \cdot dT}{dr} \tag{15}$$

The calculation of heat transfer by conduction in the pipe can be reformulated to:

$$\frac{q}{L} = \frac{k \cdot 2 \cdot \pi \cdot dT}{ln_r} \tag{16}$$

The heat flow by convection between the pipe wall and the fluid is based on Newton's law of cooling:

$$q = hA \cdot dT \tag{17}$$

Thus, to calculate heat transfer by convection in pipe can be described as:

$$\frac{q}{L} = h \cdot 2 \cdot \pi \cdot r \cdot dT \tag{18}$$

where q = Heat conduction (W);
k = Thermal conductivity (W/m°C);
r = Pipe radius (m); and
h = Convection heat transfer coefficient (W/m°C).

The heat transfer value in the pipe with insulating material can be calculated by $q_{in} = q_{out}$ (Dutta, 2004):

$$q = hi \cdot A \cdot (T_{in} - T_1) = ho \cdot A \cdot (T_4 - T_0) \quad (19)$$

Calculating the overall heat transfer on a cylinder plane inside and outside the pipe as in Figure 6 is conducted by dividing the temperature difference by the total thermal resistance between two surfaces (Ohms law):

$$\frac{q}{L} = \frac{2 \cdot \pi \cdot (T_{in} - T_{out})}{\frac{1}{hi \cdot r_1} + \frac{\ln r_2/r_1}{k_1} + \frac{\ln r_3/r_2}{k_2} + \frac{\ln r_4/r_3}{k_3} + \frac{1}{ho \cdot r_4}} \quad (20)$$

$$\Delta T = \frac{q}{m \cdot Cp_l} \quad (21)$$

where ΔT = Temperature difference (°C)

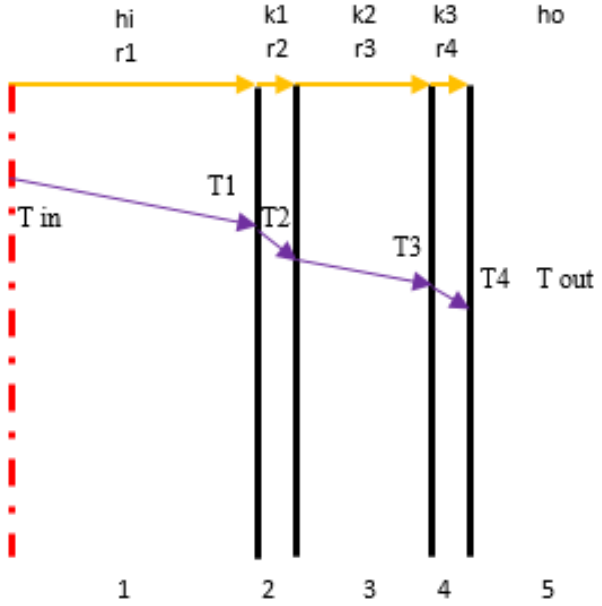

FIGURE 6: Cross section of the pipe
1) Pipe radius; 2) Pipe thickness; 3) Insulation thickness, first layer; 4) Insulation thickness, second layer; and 5) Outside air, atmospheric

The heat transfer coefficient value (Nusselt number) is calculated as described below:

$$N_{NU} = \frac{h \cdot D}{k} \quad (22)$$

The heat transfer coefficients inside and outside the pipe are:

$$h_i = \frac{N_{NU} \cdot k}{D_{in}} \quad (23)$$

$$h_o = \frac{N_{NU} \cdot k}{D_o} \quad (24)$$

Moreover, the Nusselt number outside and inside the pipe can be acquired using the Churchill/Bernstein correlation for external flow and the Dittus-Boelter correlation for internal flow:

External flow: $$NU_{Do} = 0.3 + \frac{0.62 \cdot (Re_{Do})^{0.5} \cdot (Pr)^{0.333}}{[1+ (0.4/Pr)^{2/3}]^{1/4}} \; x \left[1 + \left(\frac{Re_{Do}}{282000}\right)^{5/8}\right]^{4/5} \quad (25)$$

Internal flow $$NU_{Din} = 0.023 \cdot (Re)^{0.8} \cdot (Pr)^n \quad (26)$$

where N_{NU} = Nusselt number;
Pr = Prandtl number;
h_i/h_o = Heat transfer inside or outside pipe, convection (W/m^{2}K);
n = 0.4 for the fluid being heated and 0.3 for the fluid being cooled;
$Cp_{a/l}$ = Specific heat of air or liquid (J/kgK);
$NU_{DO/in}$ = Nusselt number outside/inside pipe;
v = Kinematic viscosity, μ/ρ (m^2/s).

3.4 Micro hydro power turbines

The types of micro hydro power generation turbine are varied, but their working principle is similar. The main working principle of a micro hydro power turbine is to extract the most energy of the water that passes its turbine blades/water wheel. The efficiency of the water wheel determines the amount of mechanical energy or shaft energy that rotates the electric generator. Hydro power energy is the combination of water flow and height difference. The continuous flow of water in a hydro system presents a stable source of pressurized liquid energy. Pressurized, flowing water is a very dense resource, and hydro energy systems convert a very large percentage of the available energy into electricity because the resource is captive in a flume or penstock. Hydro power turbins are divided into two categories:

I. Reaction turbine

a. *Kaplan and propeller turbines* (Figure 7) are axial-flow reaction turbines, the specialty of this turbine is that the motion blade angle (runner) can be adjusted in order to adapt to current flow conditions or water discharge (Štěpán, 2017). The turbine selection is based on its specific speed. The Kaplan turbine has a high specific speed and works in low head conditions with large discharge. However, the Kaplan turbine is a development of the Francis turbine and has a low head range which is about 2 to 40 m in height. The energy conversion from the water potential into mechanical energy is done through the utilization of the water velocity in a turbine water wheel.

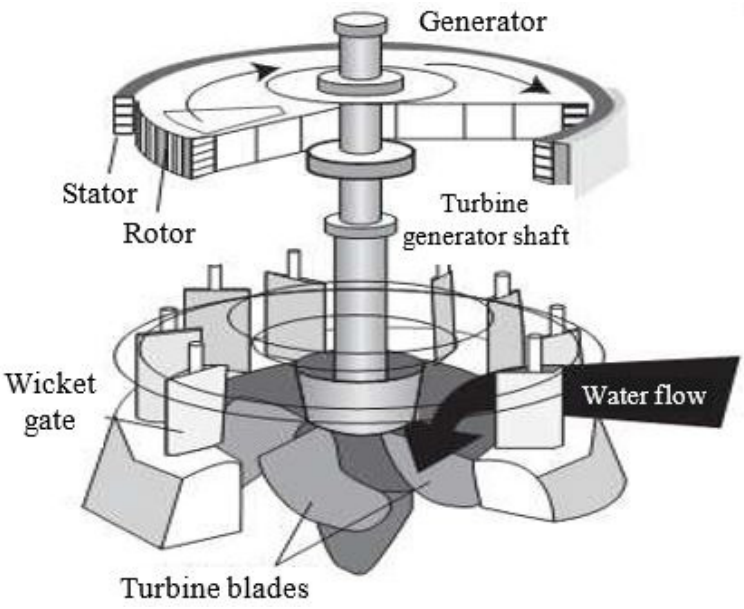

FIGURE 7: Kaplan and propeller turbine (Štěpán, 2017)

b. *The Francis turbine* has lower specific speed and works in higher head conditions with less discharge than the Kaplan or propeller turbines. The Francis turbine has a stator blade row and a rotor blade row. The stator blades can be rotated, and they are used to control flow trough the turbine. Water enters the stator blade row from a scroll as shown in Figure 8 (Mechanical booster, 2018).

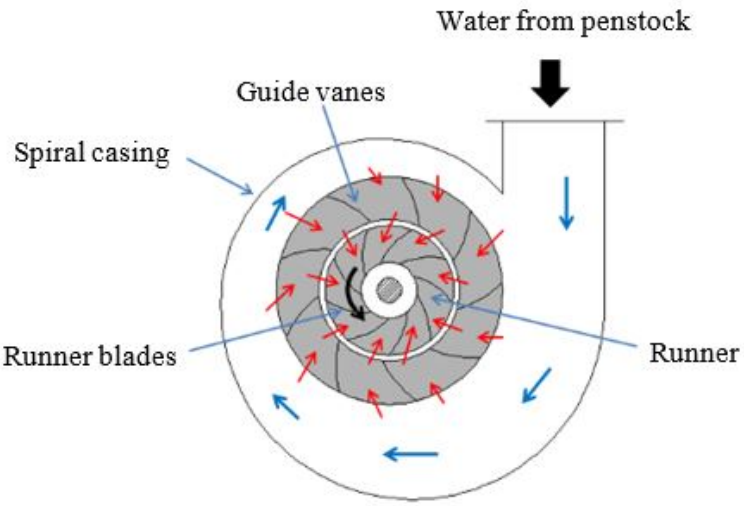

FIGURE 8: Francis turbine (Mechanical Booster, 2018)

II. Impulse turbine

a. The Pelton turbine (Figure 9) is an impulse turbine that has a free water jet coming out from nozzles. All the fluid energy in this turbine is changed to the exit velocity of the nozzle jet. The

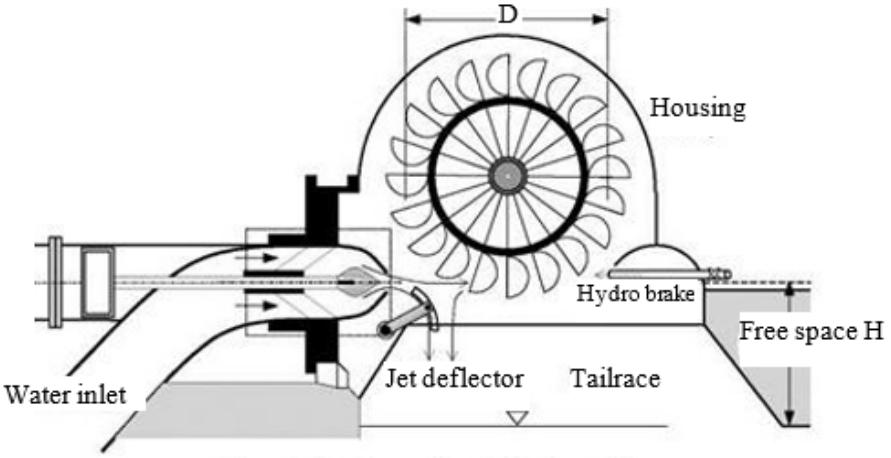

FIGURE 9: Pelton turbine (Energy Professional Symposium, 2016)

kinetic energy of the jet will be rotating the turbine wheel through buckets mounted on the wheel. (Energy professional symposium, 2016). Pelton turbines have a high efficiency where the flow is small, and the head is high.

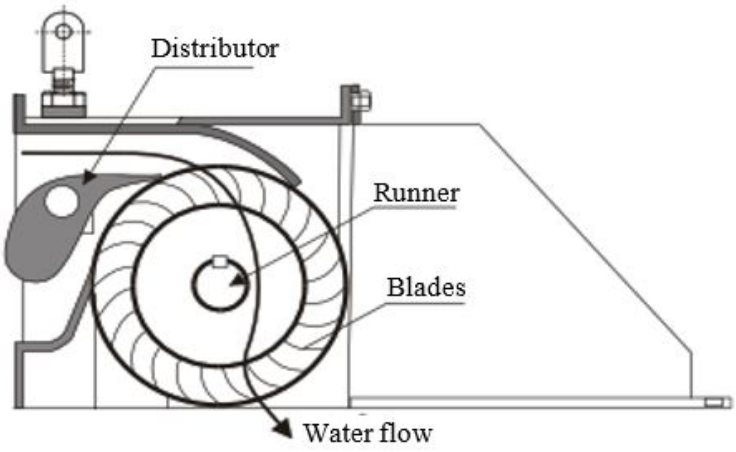

FIGURE 10: Crossflow turbine (ESHA, 2004)

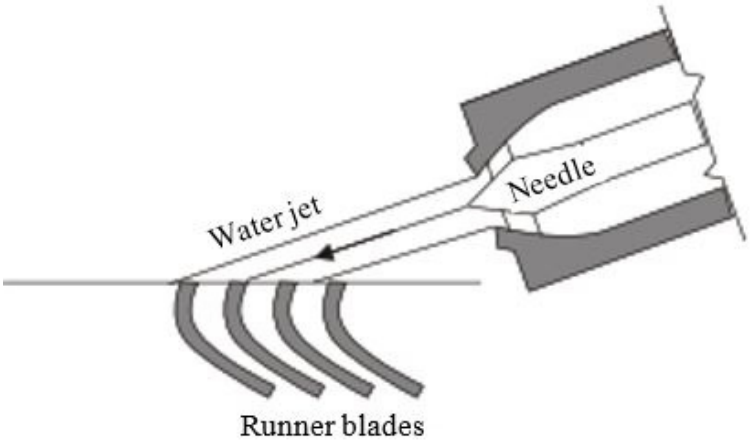

FIGURE 11: Turgo turbine (ESHA, 2004)

b. *The Crossflow turbine* (Figure 10) uses a rectangular nozzle whose width covering the full runner width. The water flows to the turbine and hits the blades where the kinetic energy is converted into mechanical energy (ESHA, 2004). The water exiting the blade row will have a second pass through the blade row on its way out of the rotor, again providing energy (lower than when entering), then leaves the turbine. The application of this turbine is high flow with a low head.

c. *The Turgo turbine* (Figure 11) is similar to the Pelton turbine and can operate at heights of 50-250 m. However, this turbine has a different bucket shape compare to the Pelton type and the water jet strikes the turbine blades at an angle of 20° (ESHA, 2004). The rotating speed of the Turgo turbine is greater than that of the Pelton turbine. As a result, it is possible to transmit energy directly from the turbine to the generator what increases total efficiency while reducing maintenance costs.

d.

As shown in Figure 12 (Tanaka Hydro, 2018), the initial stage of turbine selection considers the parameters affecting the turbine, such as:

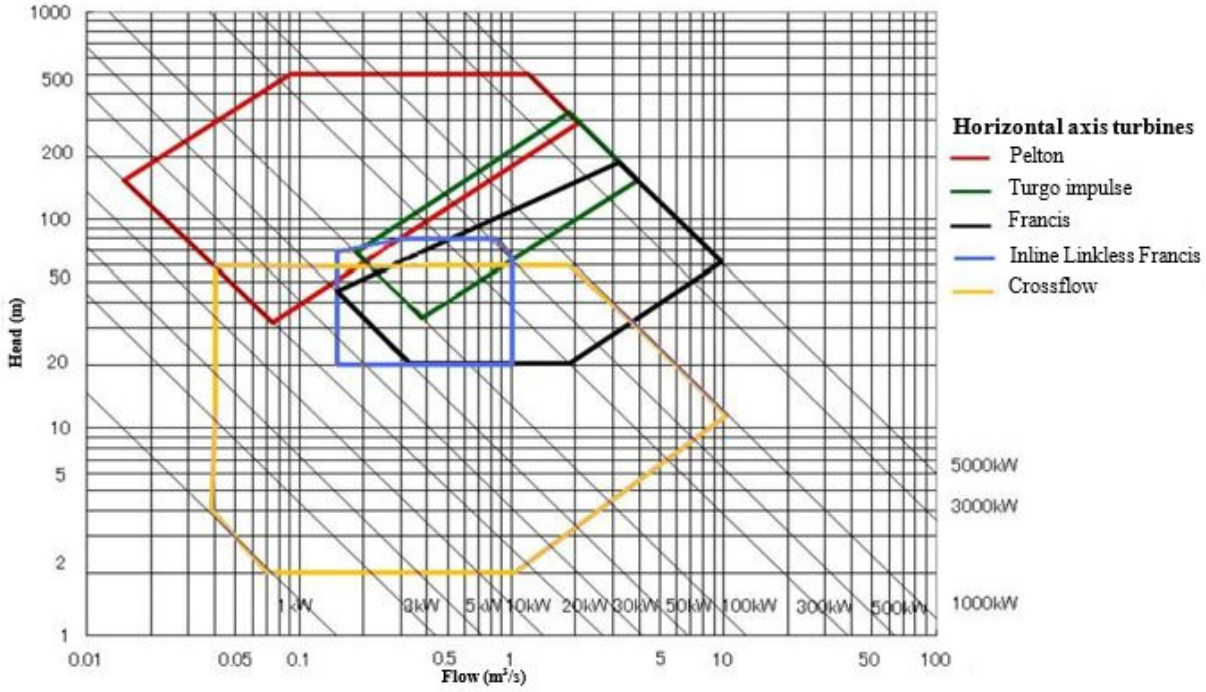

FIGURE 12: Turbine selection chart (Tanaka Hydro, 2018)

1. The effective height of water column (net head) and discharge; and
2. The desired power relates to available head and discharge.

In addition, the specific speed of the turbine (*Ns*) can also determine the suitable turbine type (Table 4).

TABLE 4: Specific speed of hydro turbine (Nair, 1984)

No.	Description	Turbine type	Ns (metric)
1.	Impuls turbine	*Pelton* One nozzle Two nozzles Four nozzles	 4 - 35 17 - 50 24 - 70
2.	Reaction turbine	*Francis* Low speed Normal speed High speed Very high speed *Propeller and Kaplan*	 80 - 120 120 - 220 220 - 350 350 - 430 300 - 1000

The hydraulic power is determined by the water flow, elevation, the height of water column (head) and the efficiency of the turbine which is can be calculated using the following equation:

$$P_h = \frac{\rho \cdot g \cdot H \cdot Q \cdot \eta}{1000} \tag{27}$$

The specific speed of the hydro turbine is formulated as follows (Finnemore and Franzini, 2011):

$$N_s = \frac{n \cdot \sqrt{P}}{H^{5/4}} \tag{28}$$

where P_h = Hydrolic power (kW);
H = Head or elevation (m);
Q = Mass flow rate (m^3/s);
η_T = Turbine efficiency (%);
Ns = Specific speed of turbine in metric (dimensionless); and
n = Tubine speed (rpm).

Then criteria for the selection of turbine type is summarized in Table 5.

TABLE 5: Operational ranges of different turbines (ESHA, 2004)

No.	Type of turbine	Head range (m)	Acceptance of flow variation	Acceptance of head variation	Best efficiency (%)
1.	*Kaplan & Propeller*	2 - 40	High	Medium-high	91-93
2.	*Francis*	25 - 350	Medium	Low	94
3.	*Pelton*	50 - 1300	High	Low	89-90
4.	*Crossflow*	5 - 200	-	-	-
5.	*Turgo*	50 - 250	Low	Low	85

In this paper we discuss the potential power generation using a Pelton turbine as an example. One characteristicof this turbine is the high head. The potential energy of water is converted into mechanical energy on the turbine wheel through an impulse process, hence the Pelton turbine is also referred to as an impulse turbine.

In order of translate the working pressure into head, the following equation is used:

$$H = P \cdot \frac{1}{0.0981 \cdot sg} \tag{29}$$

According to the standard, the absolute speed of nozzle/jet can be expressed as (Eisenring, 1991):

$$C_1 or\ V_n = k_c \cdot \sqrt{2 \cdot g \cdot H} \tag{30}$$

$$k_c = (0.96 \sim 0.98) \tag{31}$$

The optimum diameter of nozzle is:

$$d_s = \sqrt{\frac{4 \cdot Q}{\pi \cdot C_1}} \tag{32}$$

The kinetic power of the water jet can be described as follows:

$$P_k = \frac{1}{2} \cdot \rho \cdot A_n \cdot V_n^3 \tag{33}$$

where C_1/V_n = Fluids velocity in nozzle pipe (m/s).
sg = Specific gravity (ρ_f/ρ_w);
P_k = Kinetic power of water jet (kW);
k_c = Nozzle coefficient;
A_n = Cross section area of jet/nozzle pipe (m^2); and
ds = Nozzle diameter (mm).

The flow angle at the bucket entrance is β_1 and the flow angle at the exit (reflection angle) is β_2 (Modi and Seth, 1991):

$$\beta_1 = 180 - \beta_2 \tag{34}$$

$$\beta_2 = (160 \sim 170)\ ^\circ C \tag{35}$$

The circumferential speed of the turbine runner is calculated by using the following equation (Eisenring, 1991):

$$U_1 = k_u \cdot \sqrt{2 \cdot g \cdot H} \tag{36}$$

$$k_u = (0.45 \sim 0.49)$$

Turbine power which is transmitted to the bucket from water jet is calculated using Euler's equation:

$$P_t = F\ bucket \cdot U_1 = V_n \cdot A_n \cdot \rho \cdot (V_n - U_1) \cdot (1 - k \cdot cos\ \beta_2) \cdot U_1 \tag{37}$$

where β_1/β_2 = Flow angle of bucket entrance/exit (°);
U_1 = Circumferential speed of turbine runner (m/s);
k_u = Speed coefficient;
P_t = Power out of turbine (W);
F = Tangential force of bucket (N); and
k = Velocity coefficient.

3.5 Two-phase expanders (hydrothermal turbine)

To utilize hot water as a resource to generate electricity, we need to find a turbine appropriate for the two-phase working fluid. The two-phase expanders can operate with mixed fluids, that means can handle the presence of a liquid phase during expansion (wet fluids) when the fluid is in two-phase state at the expander outlet. The presence of liquid droplets does not threat to damage the machine, nor is there a risk of erosion because of the low velocities (Lemort et al., 2013). Volumetric expander types are:

1. Rotary *vane expanders* have a simple structure (Figure 13) (Zhang et al., 2014). They are chracterized by low cost, high torque and high volumetric efficiency. This expander can operate at high pressures (8 Mpa) and high temperatures (150°C). The best performance reported for vane expanders reached efficiencies of 50-80% (Żywica et al., 2016).

2. *The screw expander* (Figure 14) is a pair of helical rotors and can produce 20 kW to 1 MW with the ability to handle fluid rates from 25 to 1100 l/s (Zhang et al., 2014) while being up to 90% efficient. Screw expanders are not recommended for applications producing less than 10 kW. They can operate to 190°C as well as 1.6 Mpa (Imran et al., 2016). However, the

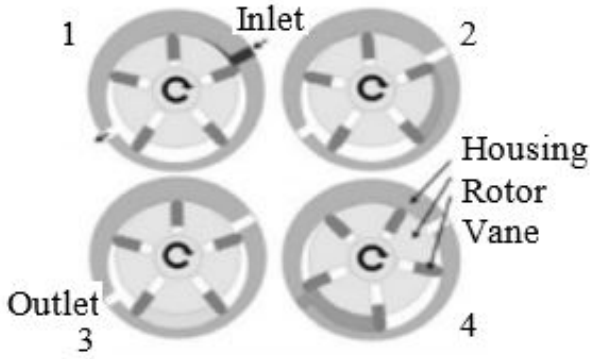

FIGURE 13: Vane expander (Zhang et al., 2014)

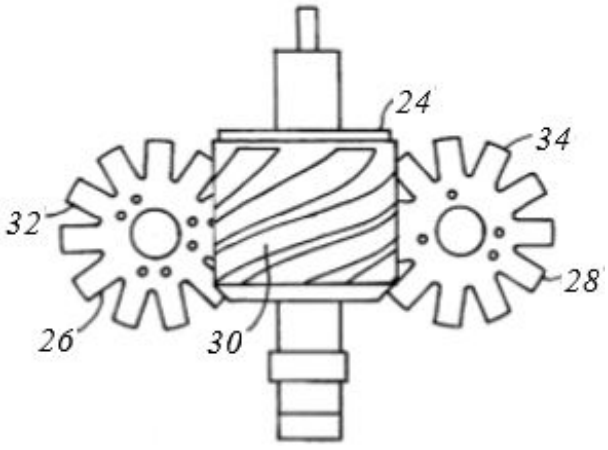

FIGURE 14: Screw expander (Öhman, 2016)

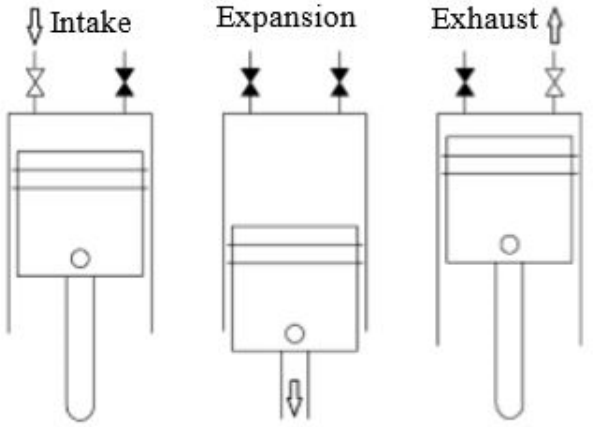

FIGURE 15: Piston expander (Żywica et al., 2016)

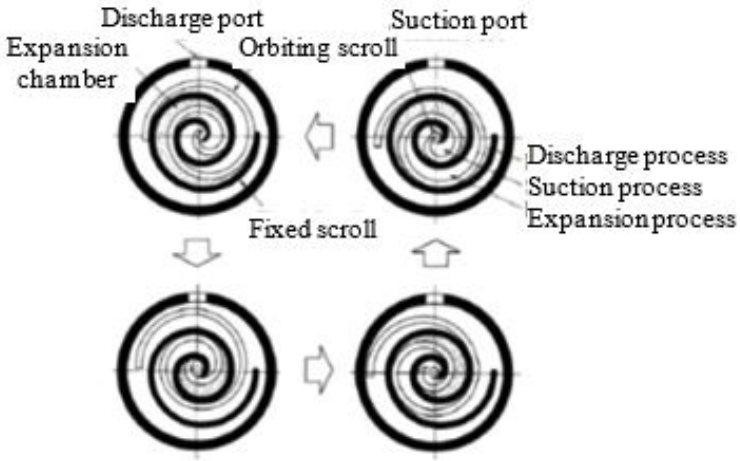

FIGURE 16: Scroll expander (Imran et al., 2016)

screw expander rotors do not get damaged if they have contact with wet steam or water and have a wider range of capacities and sizes compared to other volumetric expanders (Öhman, 2016).

3. Reciprocating *piston expander* is a positive displacement tool with three processes: intake, expansion, and exhaust step as shown in Figure 15. The maximum expander efficiency is around 40-60% (Żywica et al., 2016). Piston expanders could be operated at high pressure (9Mpa) and temperature (380-560°C) (Imran et al., 2016). The expander is not suitable for two-phase fluids which might cause damage inside the cylinder.

4. *Scroll expander* is composed of two scrolls, one is fixed and acts like a casing while the other is orbiting (Figure 16). The capability of this type is small (0.1-1 kW) (Zhang et al., 2014) and typical efficiency levels are around 80% (Żywica et al., 2016). However, reportedly this type can reach maximum power of 12 kW, the opearation pressure can reach 8.2 Mpa and the temperature 180°C (Imran et al., 2016).

5. *The turbo* or *turbine expander* (dynamic type) is suitable for power output greater than 50 kW. This type permits pressure reduction in the vapour phase but takes advantage of the buoyant and convective forces of gases released from the vapour by directing the fluid upwards such that the flow is aided by these forces (Kimmel and Cathery, 2010).

   The technology of the turbo expander has been successfully used in LNG plants, when the expansion process generates vapour and ensure remains in the liquid phase at the outlet expanders with a backpressure around 5 bar above the liquid bubble point (Kimmel, and Cathery, 2010).

An advantage of volumetric expanders is the ability to operate with a two-phase (liquid or vapour) working medium. Then, in order to select a volumetric expander, key parameters such as maximum flow rate of the fluid and the state of the fluid should be known and if the expander is able to handle two-phase mixture. A summary of various volumetric expander types is shown in Table 6.

TABLE 6: The flow rate and ability to handle two-phase mixture fluids (volumetric type)

No.	Type	Flow rate	Two-phase handling
1.	Vane expander	N/A	N/A
2.	Screw expander	25 - 1100 l/s	Yes
3.	Reciprocating piston expander	1.25 - 75 l/s	Low
4.	Scroll expander	N/A	Yes

Turbine expanders have been used for many years in the liquid natural gas (LNG) sector. A turbine expander is shown on Figure 17. The turbine expander is intended here to generate electricity from the expanding and boiling brine from the flash plant separator.

The two-phase expanders do not take vaporization of the brine into account. The efficiency is applicable to expanders (turbine) driven by boiling liquid, when boiling occurs inside the turbine (Finley, 2006).

To calculate the turbo expander efficiency, the following equation is used:

$$\eta_{one\_phase} = \frac{W_{generator\_out}}{\dot{m} \cdot (h_1 - h_2)} \quad (38)$$

When vaporization occurs, a substance exits that is partial liquid and partial vapour. The quality is definded as the ratio of the vapour mass to the total mass (mixture):

FIGURE 17: Turbo expander (Kimmel and Cathery, 2010)

$$x = \frac{m_{vapour}}{m_{total}} \quad (39)$$

$$m_{total} = m_{liquid} + m_{vapour} \quad (40)$$

The enthalpy of a two-phase fluid can be defined as:

$$h_{av} = h_f + x \cdot h_{fg} \quad (41)$$

where η_{one_phase} = Single-phase expander efficiency (%);
$\dot{m}$ = Mass flow rate (kg/s);
h_1 = Liquid enthalpy entering the expander (kJ/kg);
h_2 = Liquid enthalpy exiting the expander (kJ/kg);
x = Steam fraction (%);
h_{av} = Mixture enthalpy of saturated liquid/vapour (kJ/kg).

During the vaporization process, no work is applied to the system, thus the vapour energy term is removed from the efficiency calculation. The energy used in the vaporization process can be calculated as follows:

$$h_{vap} \cdot (x_{out} - x_{in}) \quad (42)$$

Furthermore, the useful change in enthalpy which can be transformed into shaft work is calculated as:

$$\Delta h = h_{av\_in} - [h_{av\_out} - h_{vap} \cdot (x_{out} - x_{in})] \quad (43)$$

Since h_{av_in} and h_{av_out} are the total enthalpies of the saturated mixture, this total enthalpy change is equal to the work output of an ideal 100% efficient two-phase expander. Therefore, the maximum possible work output from an ideal two-phase expander that could be converted into electricity) is:

$$W_{max} = h_{av\_in} - [h_{av\_out} - h_{vap} \cdot (x_{out} - x_{in})] \quad (44)$$

By combining the total useful change in enthalpy, the efficiency of a two-phase expander can be defined as described in Equation 45:

$$\eta_{one\_phase} = \frac{W_{generator\_out}}{\dot{m} \cdot [h_{av_{in}} - (h_{av_{out}} - h_{vap} \cdot (x_{out} - x_{in}))]} \quad (45)$$

where Δh = The useful change in enthaply (kJ/kg);
W_{max} = The maximum of work output from two-phase expander (kJ/kg);
h_{av} = Mixture enthalpy or h_m (kJ/kg);
h_{vap} = Latent heat of vaporization or h_{fg} (kJ/kg);
x_{out} = The quality of saturated mixtures at the exit of expander (%);
x_{in} = The quality of saturated mixtures at the inlet of expander (%);
h_{av_in} = Total enthalpy of saturated mixture at the inlet of expander or h_m in (kJ/kg); and
h_{av_out} = Total enthalpy of saturated mixture at the otlet of expander or h_m out (kJ/kg).

3.6 Biphase rotary separator turbine (hydrothermal)

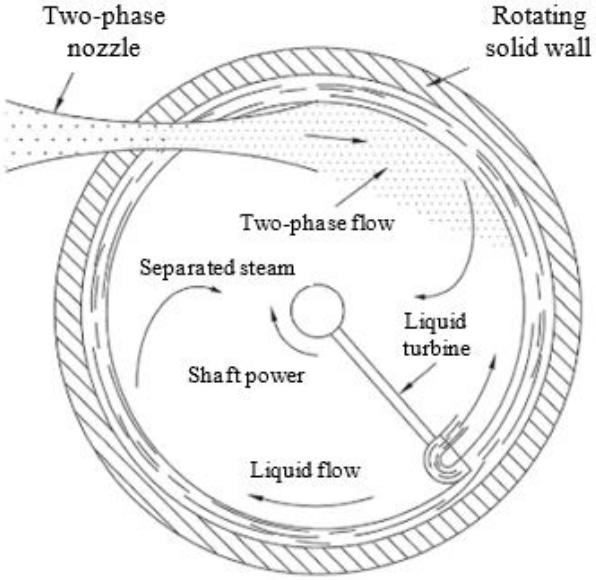

FIGURE 18: Biphase turbine (DiPippo, 2016)

The principle of biphase turbines is to replace the production separator vessel of a normal flash steam plant (geothermal plant) with a high-efficiency two-phase nozzle followed by a rotary separator. The liquid water total head was recovered to produce additional power in a Pelton-type turbine rotating in the same direction as the production separator as shown in Figure 18 (DiPippo, 2016). The biphase rotary turbine will act as a geothermal fluid separator. This separation provides additional power before the steam separates by itself and flows into the steam turbine as shown in Figure 19 (Cerini, 1978).

The biphase rotary separator turbine was more suitable than a single-flash system since its purpose was to augment the power of flash steam plant rather than to replace it. After the separation, the hot water from the biphase rotary separator tubine flows to the reinjection wells.

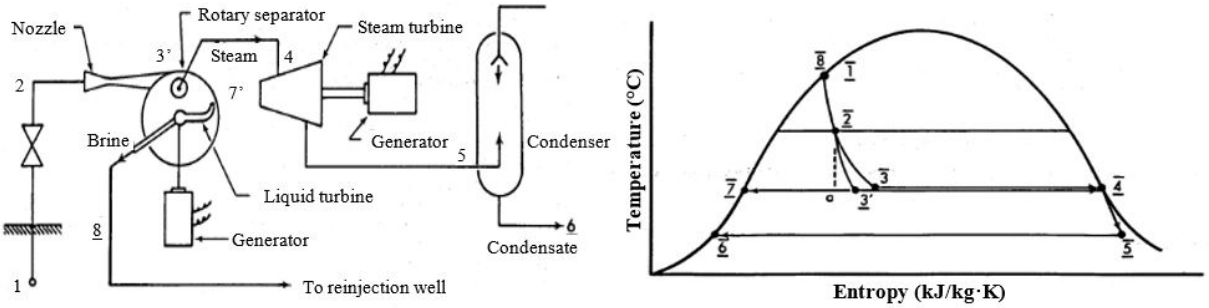

FIGURE 19: Schematic of a biphase rotary separator turbine and the TS diagram (Cerini, 1978)

The kinetic energy of the two-phase nozzle exit, and the nozzle efficiency are described using below:

$$P_n = \frac{1}{2} \cdot m \cdot {V_n}^2$$
$$\eta_n = \frac{P_n}{m_l \cdot \Delta h_i} \quad (46)$$

Then the overall efficiency can be found by:

$$\eta_o = \frac{{N_s}^2 \cdot 7.773 \cdot 10^{-7}}{\Delta h_i} \tag{47}$$

or

$$\eta_o = \frac{1/2 \cdot m \cdot V^2}{m \cdot \Delta h_i} \tag{48}$$

where P_n = Kinetic energy of two-phase nozzle exit (kW);
V_n = Nozzle exit velocity (m/s);
V = Mean steam and liquid exit velocity (m/s);
m = Total input nozzle flowrate (kg/s);
η_n = Nozzle efficiency (%);
η_o = The overall efficiency (%);
m_l = Liquid flow rate (kg/s);
N_s = Specific speed (rpm);
Δh_i = Isentropic enthalpy change for expansion from nozzle inlet pressure to atmospheric pressure condition (kJ/kg).

In the steam turbine, the enthalpy is evaluated by:

$$h_n = x_n \cdot hg_n + (1 - x_n) \cdot hf_n \tag{49}$$

Then the following expression can be solved:

$$h_2^- = h_3^- \tag{50}$$

$x_{\bar{3}}$ can be expressed as:

$$x_3^- = \frac{x_2^- \cdot hg_2^- + (1 - x_2^-) \cdot hf_2^- - hf_3^-}{hg_3^- - hf_3^-} \tag{51}$$

For the rotary separator system, the nozzle exits quality ($x_{\underline{3}}$) is evaluated as an isentropic process which then defines an enthalpy change:

$$\Delta h_i = h_2 - h_i \tag{52}$$

Since the nozzle expansion is not isentropic, a nozzle isentropic efficiency is introduced as follows:

$$\Delta h_{\underline{23}} = \eta_n \cdot \Delta h_i \tag{53}$$

For the state point conditions, the isentropic enthalpy change is calculated by first evaluating the nozzle exit quality for an isentropic expansion. Then:

$$s_n = x_n \cdot sg_n + (1 - x_n) \cdot sf_n \tag{54}$$

Substitution of the state point condition yields:

$$x_{\underline{3}} = \frac{x_{\underline{2}} \cdot sg_{\underline{2}} + \left(1 - x_{\underline{2}}\right) \cdot sf_{\underline{2}} - sf_{\underline{3}}}{sg_{\underline{3}} - sf_{\underline{3}}} \tag{55}$$

The enthalpy change corresponding to the isentropic expansion is describe by evaluating the enthalpy for state points 2 and 3. Then the difference according to Equation 56 is:

$$\Delta h_i = (x_{\underline{2}} \cdot hg_2^-) + \left(\left(1 - x_{\underline{2}}\right) \cdot hf_2^-\right) - \left(x_{\underline{3}} \cdot hg_3^-\right) - \left(\left(1 - x_{\underline{3}}\right) \cdot hf_3^-\right) \tag{56}$$

The nozzle exit enthalpy is defined by subtracting the values of $\Delta h_{\underline{23}}$ from the value of $h_{\underline{2}}$ in Equation 49:

$$h_{\underline{3}} = h_{\underline{2}} - \Delta h_{\underline{23}} \tag{57}$$

At the end, we can find the rotary separator specific power output:

$$P_{RS} = \eta_o \cdot h_{\underline{23}} \cdot m \tag{58}$$

Nozzle efficiency, is expressed as:

$$P_n = 1/2 \cdot m \cdot V_n^2 \tag{59}$$

$$\eta_n = \frac{P_n}{m_l \cdot \Delta h_i} \tag{60}$$

where $x_{\underline{3}}$ = Exit quality (%);
$\Delta h_{\underline{23}}$ = Actual enthalpy change (kJ/kg);
$h_{\underline{3}}$ = Nozzle exit enthalpy (kJ/kg);
P_{RS} = Power output of rotary separator (kW);
V_n = Nozzle velocity, using continuity equation (m/s);
P_n = Kinetic energy of two-phase nozzle (W);
η_n = Nozzle isentropic efficiency (%).

3.7 Organic Rankine Cycle turbine (binary)

The binary power generation uses two liquids that have different boiling points. The liquids that comes the from geothermal reservoirs is called the primary fluid. The secondary, working fluid has a lower boiling point than the primary liquid. The heat energy from the primary fluid is used to heat the working fluid in a closed cycle, then the working fluid is evaporated to rotate the turbine. Both fluids are not mixed but separate and the heat energy from the primary fluid is transferred through heat exchangers. The hot brine from the production separator enters the evaporator and preheater to heat the working fluid until it reaches the boiling point and changes into vapour, then the vapours flows into the turbine in order to generate electricity. This scenario does not need the recuperator to heat the working fluid, the heat comes directly from the hot brine. The working principle of the ORC (Figure 20) can be defined as follows:

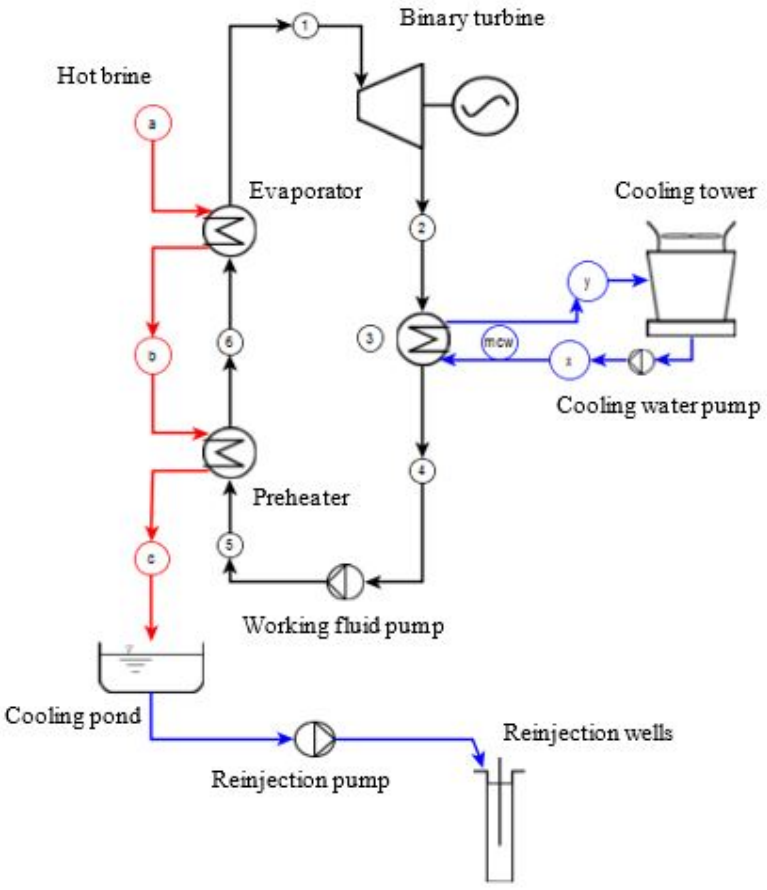

FIGURE 20: Working principle of binary turbine cycle

Process 4 - 5 : Isentropic compression in the working fluid pump;
Process 5 - 1 : Constant pressure heat addition in preheater and evaporator;
Process 1 - 2 : Isentropic expansion in the binary turbine;
Process 2 - 4 : Constant pressure heat rejection in the condenser.

Examples of candidate working fluids for ORC and their main properies are listed in Table 7.

TABLE 7: Thermodynamics, environmental and health properties of working fluids (modified from DiPippo, 2016)

No.	Fluid	Critical temp. (°C)	Critical pressure (bar)	Molar mass (kg/kmol)	Toxicity	Flammability	Ozone depletion potential	Global warming potential
1.	Propane	96.95	42.36	44.09	Low	Very high	0	3
2.	i-Butane	135.92	36.85	58.12	Low	Very high	0	3
3.	n-Butane	150.80	37.18	58.12	Low	Very high	0	3
4.	i-Pentane	187.80	34.09	72.15	Low	Very high	0	3
5.	n-Pentane	193.90	32.40	72.15	Low	Very high	0	3
6.	R-12	112.00**	41.15**	120.92**	Non-toxic	Non-flammable	1.0	4500
7.	R-114	145.70*	32.89*	170.93*	Non-toxic	Non-flammable	0.7	5850
8.	R134a	101.00*	40.59*	102.03*	Very Low	Non-flammable	0	1300
9.	R245fa	154.10*	36.40*	134.05*	Very Low	Non-flammable	0	1020
10.	Ammonia	133.65	116.27	17.03	Toxic	Lower	0	0
11.	Water	374.14	220.89	18.02**	Non-toxic	Non-flammable	0	-

Note: *Modified values by Lehr et al. (2016); **Modified values by Engineering Toolbox (2009).

3.7.1 Heat exchanger analysis: preheater and evaporator

The hot brine source is indicated in Figure 21 with point a; it represents the geothermal fluid coming from the production separator. Then the point c is the outlet of the preheater, this outlet temperature should be kept as high as possible to avoid scaling in the heat exchanger due to temperature decrease after the fluid passes through the evaporator.

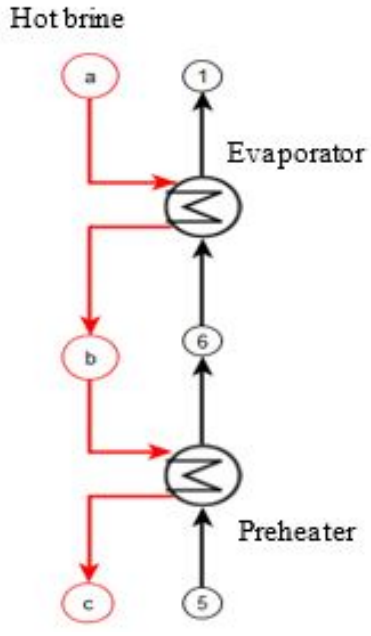

FIGURE 21: Process diagram of heat exchangers

Point 5 in Figure 21 marks where the working fluid condensate is being pumped to the preheater. The working fluids in point 6 has been heated before entering the evaporator, at the point 1 the vapour is flowinginto the turbine.

Considering the entire process as a thermodynamic system, the governing equation is:

$$\dot{m}_b \cdot (h_a - h_c) = \dot{m}_{wf} \cdot (h_1 - h_5) \quad (61)$$

If the heat capacity of the geothermal fluid is known, the left-hand side of the equation would change to:

$$\dot{m}_b \cdot \bar{c}_b \cdot (T_a - T_c) = \dot{m}_{wf} \cdot (h_1 - h_5) \quad (62)$$

Figure 22 describes the heat transfer between the geothermal fluid and the working fluid. The points a to c show how the brine temperature decreases after passing through the evaporator and preheater. The working fluid gets heated in the preheater and reaches

vapour phase after passing through the evaporator. The minimum temperature difference in the preheater and evaporator between the geothermal fluid and working fluid is called the pinch-point, and the value of that difference is the designated pinch-point temperature difference (ΔT_{pp}).

In point 5 the liquid is compressed and sub-cooled, in point 6 it is saturated at boiler pressure, and in point 1 it is saturated vapour., even with a slight superheat.

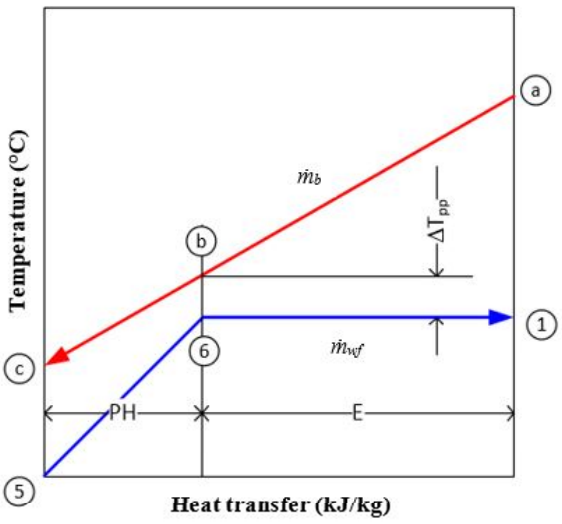

FIGURE 22: Temperature-heat transfer diagram for preheater and evaporator

Preheater:

$$\dot{m}_b \cdot \bar{c}_b \cdot (T_b - T_c) = \dot{m}_{wf} \cdot (h_6 - h_5) \quad (63)$$

Evaporator:

$$\dot{m}_b \cdot \bar{c}_b \cdot (T_a - T_b) = \dot{m}_{wf} \cdot (h_1 - h_6) \quad (64)$$

The pinch-point temperature difference is selected after an economic analysis. High price of electricity will allow large, efficient and expensive heat exchangers which translates into small pinch-point temperature differences (Dr. Páll Valdimarsson, personal comm., 2018). This allows T_b to be found from the known value for T_6 and T_c.

$$T_b = T_6 + \Delta T_{pp} \quad (65)$$

$$T_c = T_a - (T_a - T_b)\left[\frac{h_1 - h_5}{h_1 - h_6}\right] \quad (66)$$

Then the heat transferred to the working fluid is:

$$q_{in} = h_1 - h_5 \quad (67)$$

where $\dot{m}_b$ = Mass of geothermal fluid (kg/s);
$\dot{m}_{wf}$ = Mass of working fluid (kg/s);
$h_{a\text{-}b}$ = Enthalpies at each specific point of geothermal fluid (kJ/kg);
$\bar{c}_b$ = Specific heat of geothermal fluid (kJ/(kg·°C);
T = Temperature at each specific point (°C);
ΔT_{pp} = Pinch-point temperature difference (°C); and
q_{in} = Heat transferred to the working fluid (kJ/kg).

3.7.2 Binary turbine power

The vapour phase from the evaporator runs toward the binary turbine inlet to generate electricity (state point 1 in Figure 23). At state point 2 is the turbine outlet where the process is isentropic, this means the inlet entropy is equal to the outlet entropy ($S_1 = S_2$).

In the turbine, the vapour enthalpy is the enthalpy change in an ideal turbine multiplied by the turbine isentropic efficiency. For a given working fluid, the thermodynamic properties can be found in Table 7. The desired power output determines the required working fluid mass flow rate.

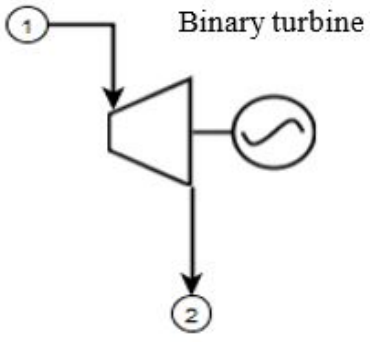

FIGURE 23: Process diagram of binary turbine

$$\dot{W}_T = \dot{m}_{wf} \cdot (h_1 - h_2) = \dot{m}_{wf} \cdot \eta_t \cdot (h_1 - h_{2S}) \quad (68)$$

where $\dot{W}_T$ = Work output (kW); and
η_t = Turbine isentropic efficiency (%).

The vapour fraction in an isentropic state. The isentropic enthalpy of the turbine and the actual enthalpy of the turbine outlet depending on the working fluid properties are described below:

$$h_2 = h_1 - \eta_T \, (h_1 - h_{2s}) \quad (69)$$

where h_{2s} = Isentropic enthalpy of working fluid (%);
η_T = Turbine efficiency (%); and
h_2 = Actual enthalpy of working fluid (kJ/kg).

3.7.3 Condenser and cooling tower type

As shown in Figure 24, the working fluid in vapour phase at point 2 will change to condensate at point 4 after passing the condenser. The condenser either works with cool air, cool water or it is a shell and tube condenser (Nugroho, 2007).

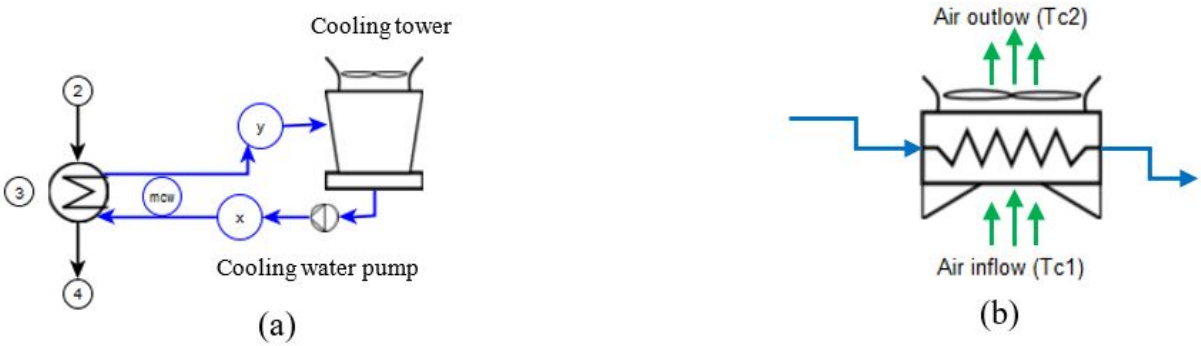

FIGURE 24: Process diagram of a) water cooling system; and b) air-cooling system

In this study, we assume a surface condenser with wet cooling tower (existing) which has the advantage that its output is less sensitive to wet bulb temperature variations. Further, air-cooled condensers are mostly used in this field due to the lack of suitable quality make-up water. Using an air-cooled condenser will significantly affect the power output, especially in the summer months, because the ambient temperature rises and of the working fluid cannot be cooled properly and high motor power is needed.

The cooling water in the condenser comes from a cooling tower or air cooler at point x, after being heated the water flows towards point y in be cooled down again. The relationship between the flow rates of the working fluid and the cooling water is:

$$\dot{m}_{cw} \cdot \bar{c} \cdot (T_y - T_x) = \dot{m}_{wf} \cdot (h_2 - h_4) \quad (70)$$

and for the air-cooled condenser type (Figure 24b):

$$\dot{m}_{air} \cdot \bar{c}_p \cdot (T_{c2} - T_{c1}) = \dot{m}_{wf} \cdot (h_2 - h_4) \quad (71)$$

where $\dot{m}_{cw}$ = Mass of cooling water (kg/s);
$\dot{m}_{air}$ = Mass of air (kg/s);
$\bar{c}$ = Specific heat capacity of cooling fluid (kJ/(kg·°C);
$\bar{c}_p$ = Specific heat capacity of dry air (kJ/(kg·°C);
T_{c1} = Temperature of the ambient air entering the cooling tower (°C); and
T_{c2} = Temperature of the ambient air leaving the cooling tower (°C).

To dissipate the required amount of waste heat, a cooling tower with a specified range, $T_y - T_x$, will need a mass flow rate determined by Equation 70. This is acceptable if the cooling water has a constant specific heat $\bar{c}$ for the small temperature range from the inlet to outlet. Furthermore, we should calculate the other parameters in the cooling system: minimum approach temperature in condenser; terminal temperature difference, condensation temperature, hot water temperature and heat rejected to the cooling tower.

$$Approach\ temperature = T_{cw} - T_{wb} \tag{72}$$

$$\Delta T_i = (11 \sim 17)°C \tag{73}$$

$$TTD = \geq 2.8°C \tag{74}$$

$$T_{cond.} = T_{cw} + \Delta T_i \tag{75}$$

$$T_{hw} = T_{cw} + Temp.increase\ of\ the\ cooling\ water \tag{76}$$

$$q_c = h_2 - h_4 \tag{77}$$

where T_{cw}/T_x = Cold water temperature (°C);
T_{wb} = Wet bulb temperature (°C);
ΔT_i = Minimum approach in condenser (°C);
TTD = Terminal temperature diagram (°C);
$T_{cond.}$ = Temperature of condensation (°C);
T_{hw}/T_y = Hot water temperature (°C); and
q_c = Heat rejected to the cooling tower (kJ/kg).

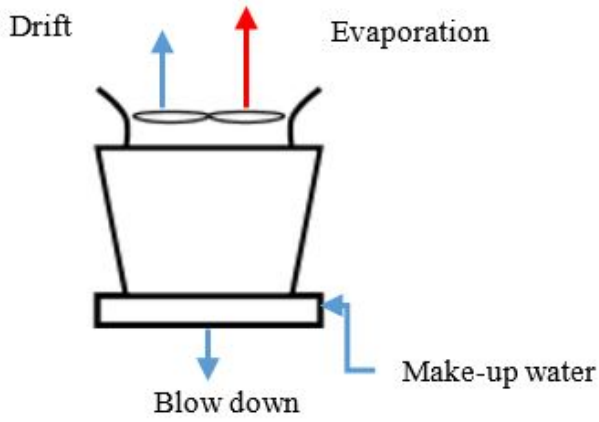

FIGURE 25: Losses in wet cooling systems

When water is used in the condenser, some water will be lost due to evaporation, drift and blow down. We need to calculate the make-up water needed (Mwagomba, 2016). There are water losses due to drift losses in droplets carried out of the cooling tower with exhaust air as seen in Figure 25, although the inflow of dry air is unchanged.

In general, the evaporation loss rate is 1-1.5% of the total circulating water, blow down is normally 20% of evaporation loss, and the drift loss is 0.03% of the total circulating water flow rate.

The dry air mass balance is:

$$\dot{m}_{a,in} = \dot{m}_{a,out} = \dot{m}_{air} \tag{78}$$

Water mass balance:

$$\dot{m}_y + \dot{m}_{a,in} \cdot \omega_{a,in} = \dot{m}_x + \dot{m}_{a,out} \cdot \omega_{a,out} \tag{79}$$

where $\dot{m}_{a,in}$ = Mass flow of cold air entering cooling system (kg/s);
$\dot{m}_{a,out}$ = Mass flow of hot air leaving cooling system (kg/s);
$\dot{m}_{air}$ = Mass flow of air used by cooling system (kg/s);
$\dot{m}_x$ = Mass flow of water leaving the cooling tower (kg/s);
$\dot{m}_y$ = Mass flow of water entering the cooling tower (kg/s);
$\omega_{a,in}$ = Specific humidity of cold air entering the cooling system (kg water/kg dry air); and
$\omega_{a,out}$ = Specific humidity of hot air leaving the cooling system (kg water/kg dry air).

The energy balance:

$$\dot{m}_y \cdot h_y + \dot{m}_{a,in} \cdot h_{a,in} = \dot{m}_x \cdot h_x + \dot{m}_{a,out} \cdot h_{a,out} \quad (80)$$

To simplify the equation, solving for $\dot{m}_a$:

$$\dot{m}_a = \frac{\dot{m}_y \cdot (h_y - h_x)}{(h_{a,out} - h_{a,in}) - (\omega_{a,out} - \omega_{a,in}) \cdot h_x} \quad (81)$$

where $h_{a,in}$ = Enthalpy of dry air entering the cooling system (kJ/kg);
$h_{a,out}$ = Enthalpy of dry air leaving the cooling system (kJ/kg);
h_x = Enthalpy of cold water leaving the cooling tower system (kJ/kg); and
h_y = Enthalpy of hot water entering the cooling tower system (kJ/kg).

The mass flow of evaporation can be defined as follows (El-Wakil, 1984):

$$\dot{m}_e = \dot{m}_{air} \cdot (\omega_{out} - \omega_{in}) \quad (82)$$

Furthermore, referring to Perry and Green (2008) formulas, the drift losses as well as blow down for mass flow and make-up water required can be calculated by the following equation:

$$\dot{m}_{drift} = 0.0002 \cdot \dot{m}_{cw} \quad (83)$$

$$\dot{m}_{bl} = \frac{\dot{m}_e - (Cycle - 1) \cdot \dot{m}_{drift}}{Cycle - 1} \quad (84)$$

$$\dot{m}_{mu} = \dot{m}_e + \dot{m}_{drift} + \dot{m}_{bl} \quad (85)$$

or referring to McDonald, (2009) approach, the blow down can be calculated using:

$$\dot{m}_{bl} = \frac{\dot{m}_e}{Cycle - 1} \quad (86)$$

where $\dot{m}_e$ = Mass flow of evaporation (kg/s);
$\dot{m}_{drift}$ = Mass flow of drift losses (kg/s);
$\dot{m}_{bl}$ = Mass flow of blow down (kg/s);
$\dot{m}_{mu}$ = Mass flow of make-up water entering the cooling system (kg/s); and
Cycle = Ratio of dissolved solids in the recirculation water to dissolved solids in make-up water, normal range between 3 to 5 cycles.

The air exit temperature for the cooling tower is therefore given by the following equation (Leeper, 1981):

$$T_{c2} = \frac{(T_y + T_x)}{2} \quad (87)$$

or

$$T_{c2} = T_{db\ or\ c1} + T_{range} \quad (88)$$

$$T_{range} = T_y - T_x \quad (89)$$

Mechanical draft type cooling tower systems, either wet or dry cooling, are most commonly in geothermal power plants. To calculate the power of the cooling tower we use the following equation:

$$\Delta P_f = \rho_{air} \cdot H_{ct} \cdot g \quad (90)$$

$$\dot{V}_{air} = \frac{\dot{m}_{air}}{\rho_{air,out}} \quad (91)$$

$$\dot{W}_{fan} = \frac{\dot{V}_{air} \cdot \Delta P_{fan}}{\eta_{fan} \cdot \eta_{motor}} \quad (92)$$

where $\dot{V}_{air}$ = Volume flow rate of air (m^3/s);
$\dot{W}_{fan}$ = Power output of fan (W);
g = Gravity, 9.81 (m/s^2);
ΔP_f = Pressure drop of fan (kg/ms^2 or Pa);
$\dot{m}_{air}$ = Mass flow of the air (kg/s);
$\rho_{air,out}$ = Air density leaving the cooling tower (kg/m^3);
η_{fan} = Fan cooling tower efficiency (%); and
η_m = Fan motor efficiency (%).

3.7.4 Feed pump and cooling water pump

The state point of the feed pump is between point 4 and 5 where the liquid has a constant density. Then we can find the isentropic enthalpy, actual enthalpy of pump as well as the cycle thermal efficiency using the following equation:

$$h_{5s} = h_4 + v_4 \cdot (P_{5s} - P_4) \cdot 100 \quad (93)$$

$$\dot{W}_p = \frac{m_{wf} \cdot (h_{5s} - h_4)}{\eta_p} \quad (94)$$

where P_4, P_{5s} = Inlet and outlet of the feed pump (kPa);
h_{5s} = Isentropic enthalpy of pump, working fluid (kJ/kg);
v_4 = Specific volume of saturation liquid, working fluid (m^3/kg);
h_{5s} = Isentropic enthalpy of pump, working fluid (kJ/kg);
η_p = Feed pump efficiency (%); and
$\dot{W}_p$ = Power output of feed pump (kW).

Furthermore, we need to install the cooling water pump between the cooling tower outlet and the condenser inlet in order to continuously transfer fresh water to the condenser and to the cooling tower. The power needed to the pump is:

$$WHP = \frac{Q \cdot H}{3960 \cdot \eta_{pump}} \quad (95)$$

where WHP = Water horsepower (hp);
H = Pump head (m); and
Q = Volume flow rate (gpm).

Leeper (1981) suggests that the head for the cooling tower pump is:

$$H_{ct} = Z_{dot} + 10 \quad (96)$$

where H_{ct} = Head of cooling tower (m); and
Z_{dot} = Tower height (m).

3.8 Double flash cycle (Back-pressure turbine)

The cycle shown in Figure 26 has additional equipment such as a throttling valve in between the separator and the flasher to create a flash of saturated liquid from the separator outlet. The throttling valve's function is to create a differential pressure or pressure drop at state 2, then the two-phase fluid enters the flasher to be separated into steam and water.

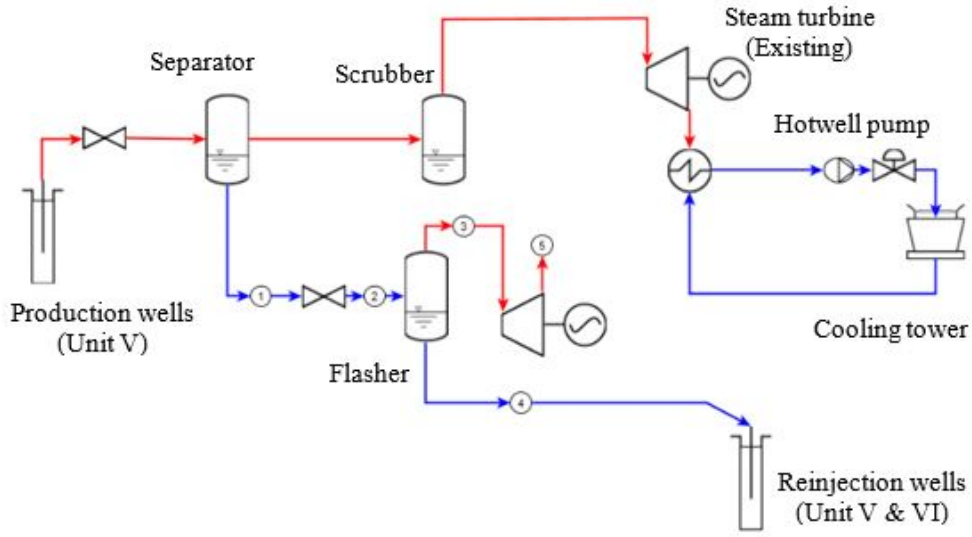

FIGURE 26: Double flash cycle

The separated steam flows towards the back-pressure turbine without condensing, and the separated water flows into the reinjection wells.

The flashing process is isenthalpic, therefore:

$$h_1 = h_2 \tag{97}$$

The steam flow enters the back-pressure turbine:

$$\dot{m}_3 = \dot{m}_2 \cdot x_2 \tag{98}$$

The steam fraction of the mixture at state 2, steam flow, isentropic dryness ($s_3 = s_5$), isentropic enthalpy, power and turbine efficiency can be calculated from:

$$x_2 = \frac{h_2 - h_4}{h_3 - h_4} \tag{99}$$

$$\dot{m}_3 = \dot{m}_2 \cdot x_2 \tag{100}$$

$$x_3 = \frac{s_5 - s_{f5}}{s_{g5} - s_{f5}} \tag{101}$$

$$h_5 = h_{f5} + x_3 \cdot \left(h_{g5} - h_{f5}\right) \tag{102}$$

$$\dot{W}_{turbine} = \dot{m}_v \cdot \left(h_{g3} - h_4\right) \tag{103}$$

$$\dot{W}_{turbine} = \dot{m}_v \cdot \eta_T \cdot \left(h_{g3} - h_4\right) \tag{104}$$

3.9 Silica saturation index (SSI)

Silica scaling inside the pipes affects the operation and production of geothermal utilization activities. Some parameters of the brine such as *pH*, temperature, pressure, silicon dioxide (SiO_2) and chloride (Cl^-) concentrations mostly influence the value of the silica saturation index. In order to know if silica scaling could occur or not inside the pipe, the silica saturation index value at operation conditions must be found. Scaling can occur if the *SSI* more than 1 and if the *SSI* is equal to 1, that means silica is in equilibrium.

According to Fournier and Rowe (1977), the solubility of amorphous silica in water can be obtained with:

$$log\ s_o = 4.52 - \left(\frac{731}{T\ (Kelvin)}\right) \quad (105)$$

4. RESULTS

4.1 Pipe size selection

The selected parameters for the calculation are based on the operation/production data and tracer flow test results of Unit V.:

Atmospheric pressure = 0.924 bar-a;
Separator pressure = 7.676 barg;
= 8.6 bar-a; and
Total flow rate of brine = 779.4 ton/hr or 216.5 kg/s (LHD-27, LHD-31, LHD-34).

From the separator pressure and the steam table we can acquire the physical properties of fluids as listed in Table 8.

TABLE 8: Material and physical properties of main pipeline

No.	Description	Value	Unit
1.	*Brine pipe (existing line):*		
	Normal pipe size	16	"
	Schedule	20	-
	Outlet diameter	0.406	m
	Inside diameter	0.390	m
2.	*Cross sectional area (A)*	0.120	m^2
3.	*Brine density (ρ_f)*	893.92	kg/m^3
4.	*Brine velocity (V_f)*	2.02	m/s

The new pipeline that will be attached to the main line is chosen to be size 6" schedule 40 with an inlet diameter of 0.15406 m. Using Bernoulli's principle, we can define the upstream pressure in the new pipe as a liquid transport to the hydrothermal turbine:

$$P_1 - P_2 = \frac{1}{2} \cdot 893.92 \cdot (2.44^2 - 2.02^2) + 893.92 \cdot 9.81 \cdot (0.15 - 2)$$

$$P_2 = 782991.90\ Pa = 7.83\ barg$$

Then, from the pressure above, we can find the velocity, minimum thickness of the pipe accordance to ASME (2000a) standard, and other physical properties (Table 9).

To calculate the flow rate inside a 6" schedule 40 pipe, we use the liquid density at working pressure 8.75 bar-a, that is 893.14 kg/m^3. The thickness the 6" schedule 40 pipe is greater than the minimum thickness needed (7.11 mm > 3.43 mm) that ensures that the pipe withstands corrosion assuming a lifetime of 30 years. The pipe size is chosen to accommodate a flow rate of 40.62 kg/s ofthe total of mass flow of 216.5 kg/s.

TABLE 9: Material and physical properties of new pipeline

No.	Description	Value	Unit
1.	*Brine pipe selection (modification line):*		
	Normal pipe size	6	“
	Schedule	40	-
	Outside diameter	0.168	m
	Inside diameter	0.154	m
2.	Cross sectional area (A)	0.0186	m^2
3.	Brine velocity (V_f) - fully liquid	2.44	m/s
4.	Gravity	9.81	m/s^2
5.	Main pipeline to the ground (h_1) - by design	2	m
6.	New pipeline to the ground (h_2) - by design	0.15	m
7.	Flow rate inside pipe 6” schedule 40	40.62	kg/s
Pipe thickness - API 5L Grade B, Carbon steel materials			
1.	Working pressure	8.75	bar-a
2.	Allowable stress (S)	20000	Psi
3.	Material coefficient (Y)	0.4	
4.	Joint efficiency (E)	1	
5.	Corrosion allowance (CA) - 30 years	3	mm
6.	Required thickness (t_r) - by pressure and temperature	0.43	mm
7.	Minimum thickness (t_m) - by pressure and temperature	3.43	mm
8.	Wall thickness of 6” schedule 40	7.11	mm

4.2 Pressure drop along new pipeline

In order to calculate the pressure, drop that will occurr in the pipeline system, it must be known what materials will be installed in the system. The planned length of the pipe is 30 m and the other materials are listed in Table 10 below adding the equivalent length of valves and fittings (L_e), values are taken from Nayyar (2000).

TABLE 10: List of material in the new pipeline system (modification)

No.	Description	Quantity	Unit	Le (ft)	Le (m)	k = Le/D
1.	Pipe, per 6 m	5	joint	-	-	-
2.	Tee reducer	1	pcs	16	4.88	31.66
3.	Standard elbow 90°	1	pcs	16	4.88	31.66
4.	Concentric reducer 6” × 1 ½”	1	pcs	15	4.57	29.68
5.	Gate valve 6” #300, fully open	2	pcs	7	2.13	13.85

The working pressure (upstream side) is 8.75 bar-a, then the physical properties of the liquid such as Reynolds number, friction factor, equivalent length and friction head related to obtain pressure drop can be calculated (Table 11).

So, from the resulte above we can obtained the pressure drop from upstream to downstream along the new pipeline which is 0.13 bar. The downstream pressure is 7.83 barg - 0.13 barg = 7.70 barg or equal to 8.63 bar-a.

TABLE 11: Physical properties and pressure drop in pipeline system

No.	Description	Value	Unit
1.	Liquid density (ρ_f)	893.14	kg/m^3
2.	Viscosity (μ_f)	155.47·10^{-6}	kg/ms
3.	Reynolds number (Re_L)	2 159 456.9	-
4.	Absolute roughness (Є) - commercial steel pipe	1.5·10^{-4} 4.57·10^{-5}	Ft m
5.	Friction factor (f), Swanee-Jain approach	0.01533	-
6.	Total equivalent length (L_e)	48.59	m
7.	Friction head (H_f)	1.47	m
8.	Pressure drop (ΔP_f)	0.13	bar

4.3 Heat loss along new pipeline

Using a working pressure of 7.83 barg or 8.75 bar-a, the physical properties of the liquid are:

Specific heat capacity (Cp_f) = 4.38 kJ/(kg·K);
Thermal conductivity (k_f) = 0.6771 W/(m·K).

Then we can calculate Prandtl and Nusselt numbers as well as the internal heat transfer coefficient inside the pipe (Table 12).

TABLE 12: Prandtl number, Nusselt number, and heat transfer inside pipe (liquid media)

No.	Description	Value	Unit
1.	Prandtl number (Pr_l)	1.0066	-
2.	Nusselt number (N_{NU_Din})	2693.70	-
3.	Heat transfer coefficient (h_i)	11839.13	W/(m^2·K)

Using an average air temperature of 22.8°C or 295.95K (PT PGE, 2015), the physical properties of air can be obtained from interpolation of atmospheric table values as follows:

Specific capacity (Cp_a) = 1.00472 kJ/(kg·K);
Specific conductivity (k_a) = 2.59·10^{-5} kW/(m·K);
Average wind velocity = 0.66 m/s (PT PGE, 2015);
Air viscosity (μ_a) = 1.83·10^{-5} kg/ms;
Air density (ρ_a) = 1.1943 kg/m^3.

The pipe will have an insulation jacket to prevent heat loss that can cause the temperature to fall excessively, as well as for safety purposes. The insulation consists of two layers, a 50 mm calcium silicate layer and a 0.8 mm aluminium layer. The material properties of the insulation jackets are:

Pipe conductivity (k_1) = 67 W/(m·K);
Calcium silicate thickness = 0.05 m;
Calcium silicate conductivity (k_2) = 0.072 W/(m·K);
Aluminium sheet thickness = 8·10^{-4} m;
Aluminium sheet conductivity (k_3)= 237 W/(m·K).

The outside diameter of the pipe including the insulation jackets is:

$$D_{o\_insulation} = 0.16828 + (2 \cdot 0.05) + (2 \cdot 0.0008) = 0.26988\, m$$

From the physical properties above, then we can estimate the Prandtl and Nusselt numbers as well as the external heat transfer coefficient outside the pipe (Table 13).

TABLE 13: Prandtl number, Nusselt number, and heat transfer outside pipe (air media)

No.	Description	Value	Unit
1.	Kinematic viscosity (*v*a) - μ/ρ	$1.529 \cdot 10^{-5}$	m^2/s
2.	Reynolds number (Re_{DO}) - air properties	11647.83	-
3.	Prandtl number (Pr_{DO})	0.7079	-
4.	Nusselt number (N_{NU_Do})	43.423	-
5.	Heat transfer coefficient (h_o)	4.171	$W/(m^2 \cdot K)$
6.	Saturation temp. (T_s) at P = 8.75 bar-a	174.18	°C

Next, we can calculate the heat loss along the new pipeline:

$$q = \frac{2 \cdot \pi \cdot (174.18 - 22.8) \cdot 30}{\frac{1}{11840 \cdot 0.077} + \frac{\ln 0.0841/0.0770}{67} + \frac{\ln 0.134/0.0841}{0.072} + \frac{\ln 0.135/0.134}{237} + \frac{1}{4.171 \cdot 0.135}}$$

$$q = 3455.87\ W\ or\ J/s$$

$$\Delta T = \frac{3456}{40.62 \cdot 4384} = 0.019\ ℃$$

The resulting temperature at the downstream end is 174.18 - 0.019 = 174.16°C.

4.4 Micro hydro and hydrothermal power

4.4.1 Micro hydro turbine power

On a potential micro hydro power site, the head value is the vertical distance of the waterfall and is usually measured in metres. Micro hydro power sites are selected based on their head and flow rate. From the calculations above, we know that the downstream pressure inside a 6-inch pipe is 7.70 barg and we calculate the head to be 87.86 m.

Furthermore, to determine the micro hydro turbine type, we need to calculate the hydraulic power and specific speed value using Equations 27 and 28 which are 25.2 and 28.01 kW, respectively. According to the turbine selection chart and specific speed, the micro hydro turbine that is best suitable is the Pelton type with one jet/nozzle. The expected power output from the Pelton turbine can be estimated (Table 14).

We assume no flashing from working temperature 174.16°C to the atmospheric temperature during the operation or in other words, the steam fraction is zero. So, the power output from the Pelton turbine is 32.04 kW with a working pressure of 7.7 barg and a liquid flow rate of 40.62 kg/s.

4.4.2 Hydrothermal turbine power (Turbo expanders)

The hydrothermal turbine will cover the expansion process associated with generating power, that means the saturated liquid pressure will be reduced what will cause the fluids to vapourise. The expansion of saturated liquid or wet vapours can be handled by turbo expanders, and if this type of expander is applicable depends on the flow rate.

The turbo expander type is selected here because the liquid is boiling. First, we calculate the power output and secondly, the efficiency of a two-phase expander utilizing the change in internal energy of the operating fluid while considering the enthalpy of vaporization. Using Equations 38-45, the results listed in Table 15 are found.

TABLE 14: Power output of Pelton turbine

No.	Description	Value	Unit	Note
1.	Upstream pressure (P_1)	7.83	bar-g	-
2.	Downstream pressure (P_2)	7.70	bar-g	-
3.	Brine density	893.79	kg/m^3	at pressure = 7.70 barg
4.	Specific gravity (sg)	0.89	-	-
5.	Head (H)	87.86	m	Converted pressure to head
6.	Flow rate (Q)	0.04	m^3/s	-
7.	Efficiency (η)	80	%	Assumed
8.	Speed (n)	1500	rpm	Assumed
9.	Hydraulic power (P_h)	25.20	kW	Before entering nozzle
10.	Specific speed (Ns)	28.01	-	With 1 jet/nozzle
11.	Absolute velocity of nozzle (C_1 or V_n)	40.69	m/s	k_c = 0.98
12.	Optimum diameter of nozzle (ds)	1.41	“	Chosen size 1 ½” schedule 80
13.	Cross section area of nozzle pipe (A_n)	0.001134	m^2	D_{in} = 0.038 m
14.	Kinetic power of water jet (P_k)	34.14	kW	-
15.	Flow angle at the bucket exit (β_2)	160	°	β_2 = 160° - 170°
16.	Flow angle at the bucket entrance (β_1)	20	°	β_1 = 180 - β_2
17.	Circumferential speed of turbine runner (U_1)	20.34	m/s	k_u = 0.49
18.	Power output of turbine (P_t)	32.06	kW	Including losses in the nozzle

TABLE 15: The physical properties of turbo expander

No.	Description	Value	Unit	Note
Flashing along pipe 6”				
1.	Upstream pressure (P_0)	8.75	bar-a	
2.	Enthalpy of sat. liquid (h_{f0})	737.56	kJ/kg	
Flashing inside turbo expander				
3.	Downstream pressure (P_1) - inlet	8.63	bar-a	
4.	Enthalpy of sat. liquid (h_{f1})	734.82	kJ/kg	
5.	Enthalpy of sat. vapour (h_{g1})	2771.35	kJ/kg	
6.	Entropy of sat. vapour (s_1 or s_{g1})	6.64	kJ/(kg·K)	$s_1 = s_{g1} = s_2$ (isentropic process)
7.	Latent heat of evaporation (h_{fg1} or h_{vap})	2036.53	kJ/kg	
8.	Atmospheric pressure (P_{atm})	0.924	bar-a	
9.	Outlet pressure (P_2) - outlet	5.924	bar-a	Kimmel and Cathery (2010)
10.	Enthalpy of sat. liquid (h_{f2})	668.34	kJ/kg	
11.	Enthalpy of sat. vapour (h_{g2})	2755.58	kJ/kg	
12.	Latent heat evaporation (h_{fg2} or h_{vap})	2087.24	kJ/kg	
13.	Entropy of sat. liquid (s_{f2})	1.93	kJ/(kg·K)	
14.	Entropy of sat. vapour (s_{g2})	6.76	kJ/(kg·K)	
15.	Proportion of flash steam (x_1) - inlet	0.13	%	Inside pipe and expander
16.	Dryness (x_2) - outlet	97.36	%	Outlet press. isentropic ($S_1 = S_2$)

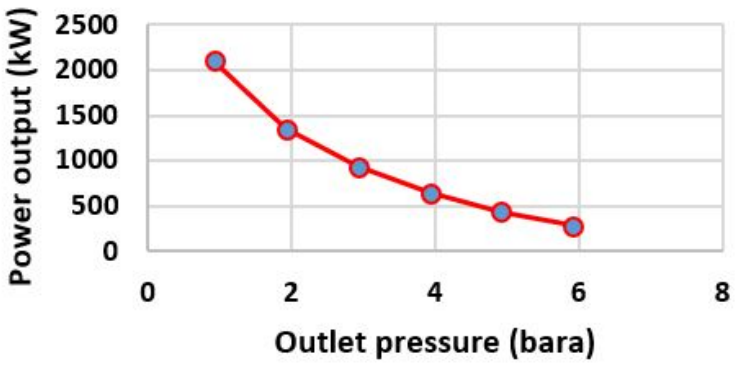

FIGURE 27: Turbo expander optimization

The fluid has around 0.13% steam when entering the expander. This happens due to pressure drop inside the 6” pipe between the separator and the expander. The steam when exiting the turbo expander is about 97.36%. There is an optimmal back-pressure of 5 bar which minimizes vapourization during the expansion process in the turbo expander.

Figure 27 illustrates how the low outlet pressure can obtain high

power but will have more boiling in the expander. The power output is shown in Table 16.

TABLE 16: The power output of a turbo expander

No.	Description	Value	Unit	Note
1.	Total flow rate (m_{tot})	40.62	kg/s	During entrance to the turbo expander
2.	Vapour flow rate (m_v)	0.05	kg/s	
3.	Liquid flow rate (m_l)	40.57	kg/s	
4.	Mixture enthalpy (h_m or h_{av}) – inlet	737.56	kJ/kg	
5.	Mixture enthalpy (h_m or h_{av}) – outlet	2700.50	kJ/kg	
6.	The energy used in vaporization process	1980.05	kJ/kg	
7.	The useful change in enthalpy (Δh) *or equal to:*	17.10	kJ/kg	
8.	Work output of turbo expander (W_{max})	17.10	kJ/kg	
9.	Power output (W generator out)	694.74	kW	Ideal power output
10.	Efficiency (η)	40.62	%	
11.	Power output	282.23	kW	The actual power output

The power output from the turbo expander is 282.23 kW with 40.62% efficiency. The power is obtained just from the liquid enthalpy, not including the vapour phase inside the expander. So, the efficiency could not be much higher.

4.4.3 Hydrothermal turbine power (biphase rotary separator turbine)

In principle, the biphase turbine works like a Pelton turbine (Table 17), but the process is similar to the

TABLE 17: The thermodynamic process of a biphase turbine

No.	Description	Value	Unit	Note
1.	Inlet pressure (P_{in})	8.63	bar-a	
2.	Atmospheric pressure (P_{out})	0.924	bar-a	
3.	Steam quality (x_2)	0.13	%	Inlet condition
4.	Total flow rate (m_{tot})	40.62	kg/s	
5.	Vapour flow rate (m_v)	0.05	kg/s	
6.	Liquid flow rate (m_l)	40.57	kg/s	
Dryness at outlet condition				
1.	Entropy of sat. vapour (s_{g2})	6.64	kJ/(kg·K)	Inlet condition
2.	Entropy of sat. liquid (s_{f2})	2.08	kJ/(kg·K)	
3.	Entropy of sat. vapour (s_{g3})	7.39	kJ/(kg·K)	Outlet condition
4.	Entropy of sat. liquid (s_{f3})	1.28	kJ/(kg·K)	
5.	Steam quality (x_3)	13.18	%	
The enthalpy change				
1.	Enthalpy of sat. vapour (h_{g2})	2771.35	kJ/kg	
2.	Enthalpy of sat. liquid (h_{f2})	734.82	kJ/kg	
3.	Enthalpy of sat. vapour (h_{g3})	2671.47	kJ/kg	
4.	Enthalpy of sat. liquid (h_{f3})	408.18	kJ/kg	
5.	The enthalpy change (Δh_i)	30.97	kJ/kg	
The actual enthalpy				
1.	Nozzle velocity (V_n)	40.69	m/s	Pipe 1 ½" sch. 80
2.	Kinetic energy of two-phase nozzle (P_n)	33.63	kW	
3.	Nozzle efficiency (η_n)	2.68	%	Pipe 1 ½" sch. 80
4.	Actual enthalpy change (Δh_{23})	0.83	kJ/kg	
5.	Expansion enthalpy (h_2)	737.56	kJ/kg	
6.	Nozzle exit enthalpy (h_3)	736.73	kJ/kg	
7.	Overall efficiency (η_o)	26.73	%	
8.	Power output (P_{RS})	9	kW	

turbo expander. The main reason to use the biphase turbine is to substitute the production separator in the geothermal field. In this case the turbine functions as a secondary power generator and the production separator is used to separate the fluids from the wells.

The nozzle velocity we use is the absolute nozzle velocity that was defined previously in micro hydro calculation results above. However, we need to find the enthalpy during each phase in order to obtain the differential enthalpies between stages. The thermodynamic process and results are listed in Table 17.

The biphase turbine has a power output of around 9 kW due to low nozzle efficiency of 2.68%. Therefore, the nozzle is replaced with a 1 ½" pipe schedule 80. This improves the nozzle velocity, but the total weight and composition of the material must be considered in the entire process.

4.5 Organic Rankine cycle (ORC) power (binary)

The selection of a suitable working fluids for an ORC cycle depends on the working fluid critical temperature compared to the temperature of the source fluid.

First, we choose i-Pentane and assume that no pressure drop occurs in the binary cycles (heat exchangers and piping system) as well as no boiling in the brine. The initially known variables of the binary design are:

- Brine source pressure (P_a) = 8.63 bar-a;
- Brine inlet sat. temperature (T_a) = 173.56°C;
- Flow rate of brine (m_b) = 40.62 kg/s;
- Pinch point of HE ($\Delta T_{pp,in}$) = 5°C;
- Pinch point of condenser ($\Delta T_{pp,out}$) = 10°C;
- Preheater-evaporator pressure = $P_5 = P_6 = P_1$;
- Turbine isentropic efficiency (η_T) = 85% (assumed);
- Feed pump isentropic efficiency (η_p) = 75% (assumed);
- Fan isentropic efficiency (η_f) = 65% (assumed);
- Specific isobaric heat capacity ($\bar{c}_b$) = 4.38 kJ/(kg·°C) for T_a; and
- Recuperator = not used.

The working fluid pressure is set to 8.63 bar-a.

Design and optimization of binary using numerical computation

The binary power is calculated using Scilab and CoolProp. The initially known variables are:

- Fluid = Pentane
- Vaporizer pressure (P_v) = 8.63 bar-a (for SSI > 1) and 18.7 bar-a (for SSI < 1);
- Source temperature (S_1) = 173.57°C;
- Flow rate of brine (m_b) = 40.62 kg/s;
- Condensation temperature ($T_{cond.}$) = 44°C;
- Pinch point of vaporizer ($\Delta T_{pp,in}$) = 5°C;
- Pinch point of condenser ($\Delta T_{pp,out}$) = 10°C;
- Superheat temperature (T_{sh}) = 2°C;
- Boiling margin temperaure (T_{bm}) = 2°C;
- Turbine isentropic efficiency (η_T) = 85% (assumed);
- Feed pump isentropic efficiency (η_p) = 75% (assumed);
- Cooling water pump efficiency (η_{cwp}) = 75% (assumed);
- Cooling tower fan efficiency (η_f) = 65% (assumed);

- Cooling tower fan motor eff. (η_{mf}) = 75% (assumed); and
- Recuperator = not used.

A superheat of 1-2 °C and a boiling margin of similar value is assumed (Dr. Páll Valdirmarsson, personal comm., 2018).

These input values are used for the Scilab programme in order to acquire optimization of the power output with different working fluids. Results were obtained using Penthane and are described in Figure 28 (*SSI* > 1) and Figure 29 (*SSI* < 1). The main results are summarized in Table 18.

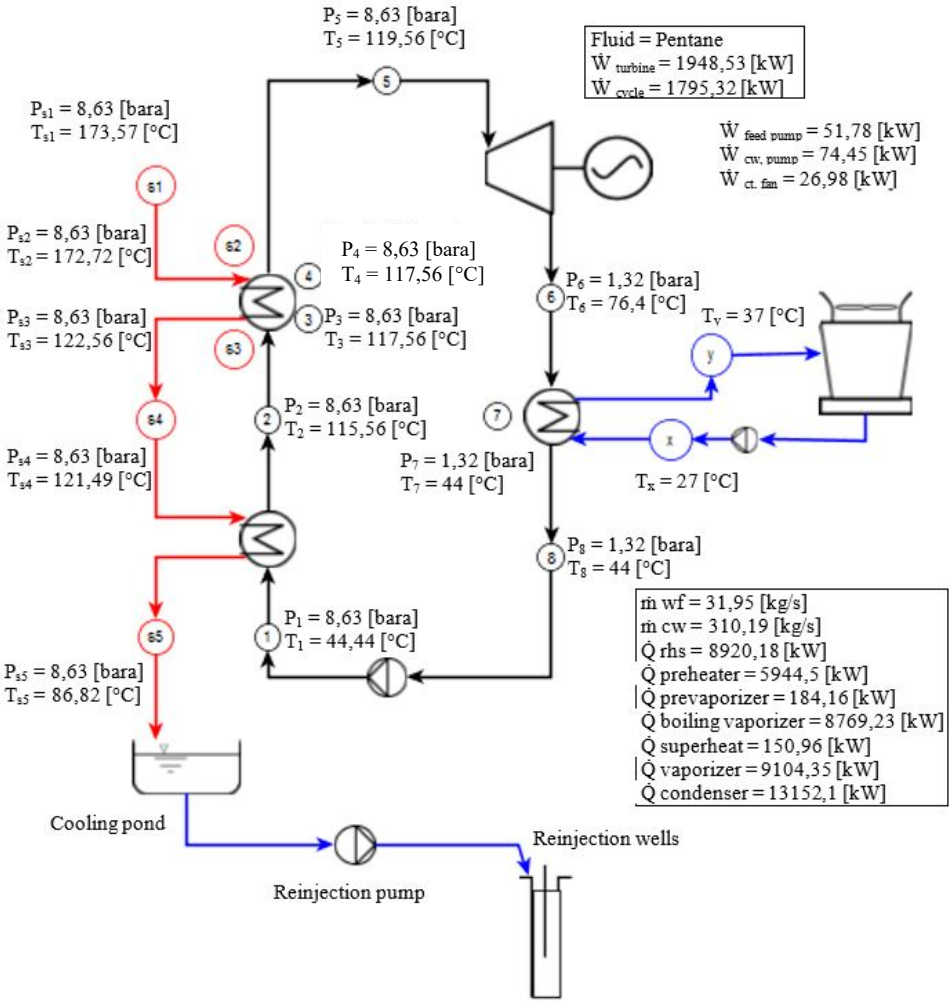

FIGURE 28: Binary cycle with SSI > 1 and wet cooling type
(calculated with Scilab and CoolProp)

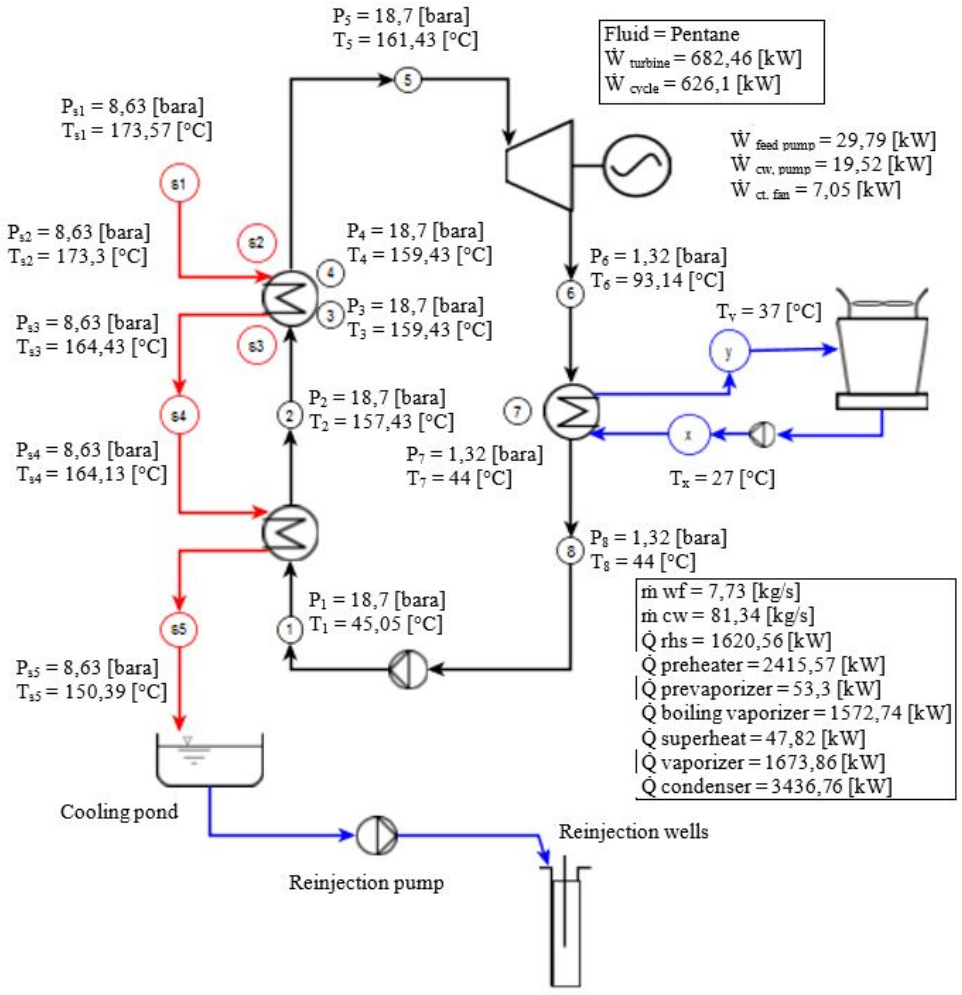

FIGURE 29: Binary cycle with SSI < 1 and wet cooling type
(calculated with Scilab and CoolProp)

4.6 Back-pressure turbine power (double-flash cycle)

In the case of a double-flash cycle, we use the entire brine flow rate from the production separator of Unit V Lahendong (around 216.5 kg/s) to be used for a back-pressure turbine. Three cases are calculated, with the pressure in the low-pressure separator (at state 2) is assumed to be 2.9 bar-a, 4.8 bar-a and 6.7 bar-a. Other assumptions are:

- No pressure drop in the steam pipe and inside flasher separator;
- No heat loss in the pipeline system;
- Flasher separator efficiency is neglected, and isentropic turbine efficiency is 85%.

Figure 30 illustrates that the optimum power output of the double-flash cycle is 2447.56 kW with a flasher separator pressure of 4.8 bar-a. The output is chosen due to consideration of the saturation temperature and working pressure on the flasher separator. The pressure may not be too low to maintain the flow of the hot brine to the reinjection wells. The *SSI* value from this cycle is 0.99 and it increases when the working pressure of the flasher separator is lower as described in Figure 31 and Figure 32.

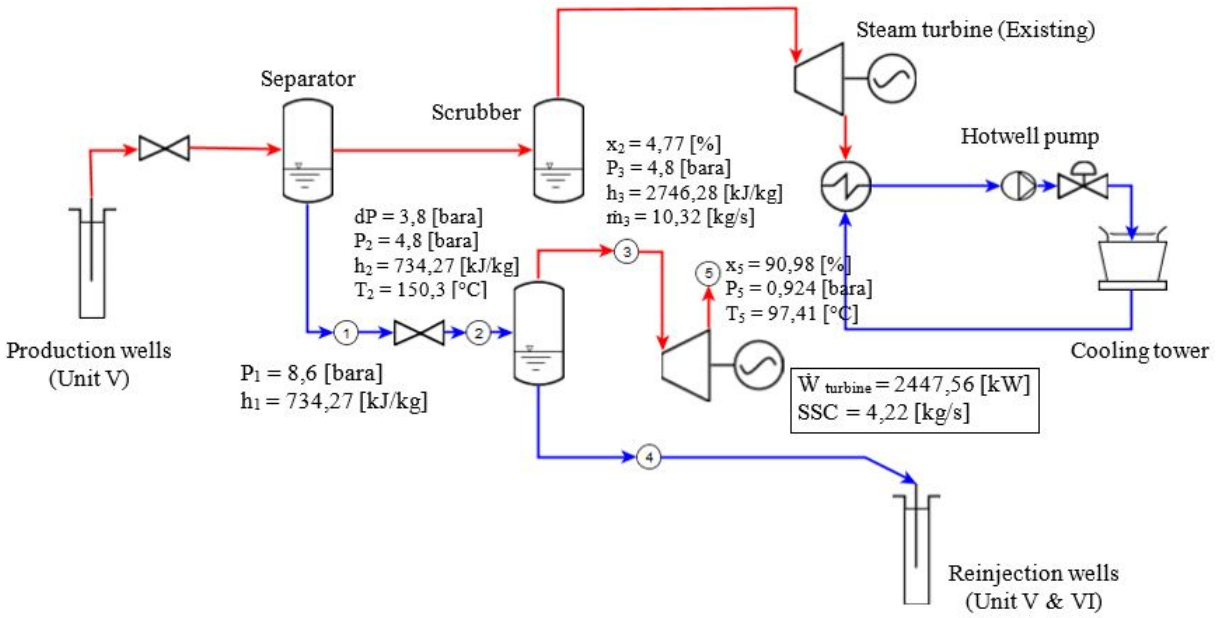

FIGURE 30: Double-flash cycle output

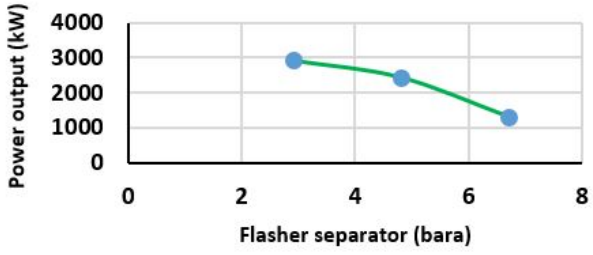

FIGURE 31: Power output vs. pressure of double-flash cycle

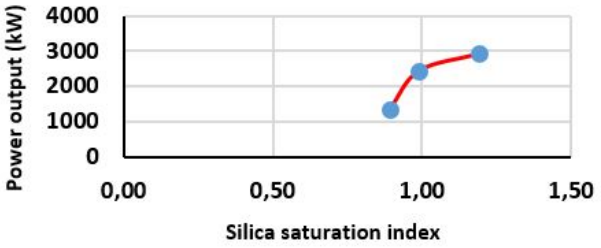

FIGURE 32: Power output vs SSI of double-flash cycle

The enthalpy of the production separator is equal to the flasher separator and since the production separator pressure has not changed (mandatory), the flasher enthalpy is equal. However, the change in pressure in the flasher separator is followed by the changes in the steam fraction and steam flow, the lower pressure obtaines the high steam fraction.

4.7 Silica saturation index

4.7.1 Silica scaling in the hydro turbine process

The laboratory test result for separator in Unit V on 25 June 2018 (PT PGE, 2018c) are:

pH = 8.6;
S_iO_2 = 620 mg/l; and
Cl^- = 705 mg/l.

This data is used to assess the potential of silica scaling in the new pipeline between the tapping line and the hydrothermal turbine inlet. Silica scaling occurs if the value of *SSI* > 1. In this pipeline system heat loss is about 0.019°C resulting in a temperature at the end of pipe of 174.16°C. We can now calculate the silica saturation index as follows (Table 19).

TABLE 19: Silica saturation index in different temperatures

No.	Desription	Value	Unit
Brine temp. = 174.18°C at upstream side			
1.	Log s_o - Fournier and Rowe (1977)	2.8859	-
	Solubility of amorphous silica in water (s_o)	768.902	mg/l
2.	D_t - Chen and Marshall equation	0.04668	-
3.	Salinity (m_{Cl})	0.0199	mol/l
4.	Silica saturation index (SSI)	0.8081	-
Brine temp. = 174.16°C at downstream side			
1.	Log s_o - Fournier and Rowe (1977)	2.8858	-
	Solubility of amorphous silica in water (s_o)	768.776	mg/l
2.	D_t - Chen and Marshall equation	0.04668	-
3.	Salinity (m_{Cl})	0.0199	mol/l
4.	Silica saturation index (SSI)	0.8082	-
Silica scaling start to formed at temperature = 150°C and below it			
1.	Log s_o - Fournier and Rowe (1977)	2.7925	-
	Solubility of amorphous silica in water (s_o)	620.126	mg/l
2.	D_t - Chen and Marshall equation	0.05095	-
3.	Salinity (m_{Cl})	0.0199	mol/l
4.	Silica saturation index (SSI)	1.0021	-

The critical *SSI* would be reached at temperature about 150°C or less (Figure 33).

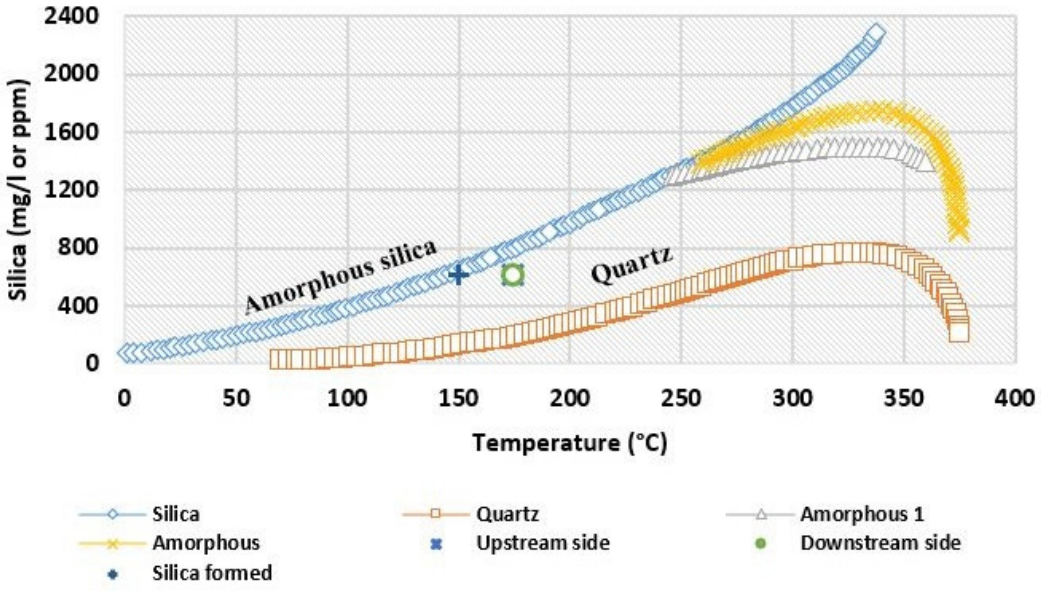

FIGURE 33: Solubility of amorphous silica vs. temperature

4.7.2 Silica scaling in binary ORC process

Similarly, we can find the *SSI* values of binary cycle process (from manual optimization). Table 20 shows the *SSI* for different working pressures and temperatures.

TABLE 20: Silica saturation index in binary ORC cycle

Desription	Pressure (bar-a)	End temp. (°C)	SSI
Binary ORC with wet or dry cooling tower	8.63 23.03	74.37 150.05	2.38 1.002

5. CONCLUSIONS

The working pressure and hot brine flow rate from the production separator in this research project is enough to install a secondary power generator. The generator could be installed during a shutdown or a production break of around 2 days. The chosen pipe size is 6" schedule 40. The primary power generation will be undisturbed.

The overall length of a new pipe is 30 m, the pressure drop inside the pipe is around 0.13 bar-g and the heat loss is 0.019°C. The downstream pressure and temperature are sufficient to run a micro hydro and hydrothermal (expander) turbine. In micro hydro design, it is assumed that there is no boiling of liquid inside the pipe. A micro hydro with Pelton type turbine will have to be located near a cooling pond and utilize cold water to mix with the brine before the turbine. The reason is that the high temperature of the brine from the separator will cause boiling inside the pipe which will affect the Pelton turbine.

The next part of the process design is using two-phase expanders and biphase turbine. A turbo expander is chosen because it has been used successfully on the LNG plant to generate power from boiling liquid. The turbo expander and the biphase turbine generate power from two-phase fluids in a similar way. It should convert vapour energy to shaft work of the turbine. The difference between them is that turbo expander has an outlet back-pressure of about 5 bar to prevent excess steam that would remain inside the turbine while the biphase turbine use atmospheric pressure for the outlet.

The common technology is to use organic fluids in binary turbines. This binary turbine uses a surface condenser (shell and tube) for the cooling process, so the working fluid does not come into direct contact with the cooling media in either the wet or dry cooling tower. The power output is about 3 to 4 times higher if we do not consider the *SSI*. The main reason forusing a dry cooling tower would be if the existing wet cooling tower in Lahendong Unit V cannot use binary cooling processes. This will influence the mass balance, require a cooling water pump, and disturb cooling tower basin maintenance activities. However, the power output of the turbine is not affected too much using a wet or dry cooling tower, but the fan power in a dry cooling tower is 4 to 5 times higher during the summer season.

From the chemistry composition of geothermal fluids in Unit V Lahendong, the minimum temperature that can be utilized for the system is 150°C to prevent silica scaling in the evaporator and preheater (heat exchanger). The limitation of temperature has a significant impact on the power production. By using a suitable working fluid (Pentane), the net power of the binary turbine that can be exported to the grid is 626.1 kW, using the existing wet cooling tower as the cooling system.

The last part in this research project was to use a back-pressure turbine as double-flash cycle system which can generate around 2450 kW. The process was optimizated considering the SSI value. The working pressure in the flasher separator is 4.8 bar-a to pump the hot brine into the reinjection wells.

6. RECOMMENDATIONS

The selection of a secondary turbine in Unit V Lahendong is dependent on available technology, operation parameters, short/long term necessity, cost and production results. Calculations indicate that a hydrothermal turbine can generate power from two-phase fluids (boiling liquid) using a turbo expander, but this needs to be tested and verified in the geothermal field.

For lighting and small power purposes like the compressor or pump in the peripheray of the Lahendong cluster, a micro hydro turbine of the Pelton type is appropriate and would reduce the monthly electricity cost. However, the working pressure to generate electricity is controlled by the pump discharge between the cooling pond and the reinjection wells.

A binary turbine with an organic working fluid is the best option to develop secondary power generation in Unit V Lahendong and other PT Pertamina Geothermal Energy fields. With the same parameters (working pressure, temperature and flow rate), a binary turbine can achieve higher power outpt than others secondary turbines and we highly recommended the use of a dry cooling tower as cooling system in order not disturb the operations and maintenance of Unit V either during shutdown or production.

However, double-flash cycle, either condensing or non-condensing types, should be taken into consideration in the next green field projects of PT Pertamina Geothermal Energy. The secondary power from this cycle would contribute to the total power production and should be part of the design at the initial project phase, so it will not interfer with operations and production activities when installed.

ACKNOWLEDGEMENTS

I would like to express my sincere gratitude to Mr. Lúdvík S. Georgsson, the Director of UNU GTP, and a very kindness person for having been granted a scholarship award for six months in Reykjavík, Iceland commencing on April 2018. My thanks also address all of UNU-GTP staff members, Ms. Thórhildur Ísberg, Ms. Málfrídur Ómarsdóttir, Mr. Markús A.G. Wilde, Mr. Ingimar G. Haraldsson, Mr. Jóhann F. Kristjánsson for their assistance and support during my studies and life in Iceland. A special thanks go to Mr. Yanuaris Dwi Cahyono, Ms. Margiet Candrikawati, Ms. Gloria Gladis Sondakh, Mr. Ren Xiaoqing, Mr. Nathaniel Mugo, and Ms. Laura de Cordero de Fuentes and UNU Fellows 2018 for their friendship and collaboration.

I want to thank also all members of PT Pertamina Geothermal Energy managements, Mr. Irfan Zainuddin, Mr. Ali Mundakir, Mr. Eko Agung Bramantyo, Mr. Khairul Rozaq, Mr. Maizar Yanto, Mr. Salvius Patangke, Mr. Ahmad Yani, Mr. Bambang Sembodo and Mr. Priatna Budiman who allowed, supported, and gave me the opportunity to study in Iceland. Furthermore, I would like to thank all of my colleagues at PT Pertamina Geothermal Energy, area Lahendong, for supporting the research project by providing data and carrying oout my daily duties during my studies in Iceland.

I have great pleasure acknowledging my gratitude to my supervisor, Prof. Dr. Páll Valdirmarsson, for his time, expertise, challenge, assistance and sharing of practical knowledge during the completion of my research project.

I owe my deepest thanks and I dedicate this goal to my parents, Mr. Sayogi and Mrs. Sri Subaningsih; my father and mother in-law, Mr. Masdoeki (Alm.) and Mrs. Imas Sulasmi; to my beloved wife and children, Mrs. Eka Wartini, Alesha Khayla Nugraha and Raffasya Kinza Nugraha who have been supporting me spiritually as well as made me a beautiful world throughout my life.

Finally, I want to express my deepest gratitude to Allah SWT, the almighty, to give me his blessing and health throughout my life as well as the ability, knowledge, and strength to achieve the objectives of the research project. Without His blessings, this achievement would not have been possible.

REFERENCES

ASME, 2000a: *Process piping*. The American Society of Mechanical Engineers, NY, USA, ASME B31.3a Addenda 335 pp.

Cerini, D.J., 1978: *Demonstration of a rotary separator for two-phase brine and steam flows*. *Final report*. The National Technical Information Services, Virginia, USA, 56 pp.

DiPippo, R., 2016: *Geothermal power plants*: *Principles*, *applications*, *case studies and environment impact* (4th ed.). Butterworth Heineman, Elsevier Ltd., Kidlington, UK, 762 pp.

Dutta, P., 2004: *Heat and mass transfer*. Indian Institute of Science Bangalore, unpublished learning material, volume 1, 334 pp.

Eisenring, M., 1991: *Micro Pelton turbines* (1st ed.). *MHPG series*: *Harnessing water power on a small scale* (vol. 9). GATE and SKAT, St. Gallen, Switzerland, 86 pp.

El-Wakil, M.M., 1984: *Power plant technology*. McGraw-Hill, Inc., USA, 859 pp.

Energy professional symposium, 2016: *Pelton turbine*. Energy professional symposium, website: *energyprofessionalsymposium.com/?p=34484*

Engineering Toolbox, 2009: *Molecular weight-common substances*. Engineering Toolbox, website: *www.engineeringtoolbox.com/molecular-weight-gas-vapor-d_1156.html*

ESHA, 2004: *Guide on how to develop a small hydropower plant*. The European Small Hydropower Association, 294 pp.

Finley, C.D., 2006: Definition of hydraulic efficiency of two-phase expanders driven by boiling liquid. *AIChE Spring Meeting*, *6th Topical Conference on Natural Gas* Utilization, Orlando, FL, 6 pp.

Finnemore, E.J., and Franzini, J.B., 2011: *Fluid mechanics with engineering applications* (10th ed.). McGraw-Hill Education Ltd., India., 816 pp.

Fournier, R.O., and Rowe, J. J., 1977: The solubility of amorphous silica in water at high temperatures and high pressures. *Am*. *Min., 62*, 1052-1056.

Imran, M., Usman, M., Park, B.S., and Lee, D.H., 2016: Volumetric expanders for low grade heat and waste heat recovery applications. *Renewable and Sustainable Energy Reviews, 57*, 1090-1109.

Jónsson, M.T., 2018: *Pipe design*. UNU-GTP, Iceland, unpublished lecture notes, 54-77.

Kimmel, H. E., and Cathery, S, 2010: Thermo fluid dynamics and design of liquid-vapour two-phase LNG expanders. *GPA paper*, 9 pp.

Lehr, J. H., Keeley, J., and Kingery, T.B., 2016: *Alternative energy and shale gas encyclopedia*. John Wiley & Sons Inc., NJ, 912 pp.

Leeper, S.A., 1981: *Wet cooling towers: rule of thumb, design and simulation*. US Department of Energy, ID, 24 pp.

Lemort, V., Ludovic, G., Arnaud, L., Declaye, S., and Quoilin, S., 2013: A comparison of piston, screw and scroll expander for small Rankine cycle systems. *Proceedings of the 3rd International Conference on Microgeneration and Related Technologies, Naples, Italy.*

Lyle, O., 1947: *The efficient use of steam* (1st ed.). Her Majesty's Stationery Office, London, England, 932 pp.

McDonald, J., 2009: *Drop by drop*, *articles on industrial water treatment* (version 3). Crown Solutions Co. LLC, 485 pp.

Mechanical Booster, 2018: *What is reaction turbine - Principle, working, main components and application*. Mechanical Booster, website: *www.mechanicalbooster.com/2018/01/reaction-turbine.html*

Modi, P.N., and Seth, S.M., 1991: *Hydraulics and fluid mechanics including hydraulic machines* (10th ed.). Standard Book House, Nai Sarak, Delhi, 1350 pp.

Mwagomba, T., 2016: *Preliminary technical and economic feasibility study of binary power plant for Chiweta geothermal field, Malawi*. Reykjavík University, MSc thesis, UNU-GTP, Iceland, report 1, 78 pp.

Nair, A.G., 1984: *Selection of turbines with special reference to Pooyankutty hydro-electric scheme complex*. University of Roorkee, MSc thesis, India, 100 pp.

Nayyar, M.L., 2000: *Piping handbook* (7th ed.). McGraw- Hill Companies, Inc., USA, 2147 pp.

Nugroho, A.J., 2007: Evaluation of waste brine utilization from LHD unit III for electricity generation in Lahendong geothermal field, Indonesia. Report 17 in: *Geothermal Training in Iceland* 2007. UNU-GTP, Iceland, 391-415.

Öhman, H., 2016: *Low temperature difference power systems and implications of multiphase screw expanders in Organic Rankine Cycles*. KTH Royal Institute of Technology, Sweden, PhD thesis, 93 pp.

Perry, B.H. and Green, D.W., 2008: *Perry's chemical engineers' handbook* (8th ed.). McGraw-Hill, Inc., New York, USA, 2735 pp.

PT PGE, 2012a: *Production test report of LHD-27 well*. PT Pertamina Geothermal Energy, Lahendong area, Indonesia, unpublished report, 40 pp.

PT PGE, 2012b: *Production test report of LHD-34 well*. PT Pertamina Geothermal Energy, Lahendong area, Indonesia, unpublished report, 55 pp.

PT PGE, 2015: *Lahendong unit 5 & 6 geothermal power project of BEDD, as built document*. PT Pertamina Geothermal Energy, Lahendong area, Indonesia, unpublished report, 25 pp.

PT PGE, 2016: *Production test report of LHD-31 well*. PT Pertamina Geothermal Energy, Lahendong area, Indonesia, unpublished report, 41 pp.

PT PGE, 2017: *Tracer flow test report of LHD cluster 27*. PT Pertamina Geothermal Energy, Lahendong area, Indonesia, unpublished report.

PT PGE, 2018a: *Operation departments*. PT Pertamina Geothermal Energy, Lahendong area, Indonesia, unpublished material.

PT PGE, 2018b: *Securing our future national energy demand with geothermal energy*. PT Pertamina Geothermal Energy, Lahendong area, Indonesia, unpublished material.

PT PGE, 2018c: *Geochemist laboratory analysis of Lahendong geothermal field*. PT Pertamina Geothermal Energy, Lahendong area, Indonesia, unpublished report.

Štěpán, J., 2017: *Determination of synchronous machine parameters*. University of West Bohemia, Pilsen, Diploma thesis, 54 pp.

Tanaka Hydro, 2018: *Tanaka Suiryoku turbine selection chart*. Tanaka Hydropower Co. Ltd., website: *www.tanakahydro.jp/products/*

Zhang, Y., Saghlatoun, S., and Zhuge, W., 2014: Review of expander selection for small-scale organic rankine cycle. *Proceedings of the ASME 4th Joint US-European* FEDSM, IL, USA, 8 pp.

Żywica, G., Kaczmarczyk, T., and Ihnatowicz, E., 2016: Expanders for dispersed power generation: maintenance and diagnostics problems. *Transactions of the IFFM No. 131*, Poland, 173-188.